

THE UNIVERSITY OF CALGARY

STUDIES IN RECOVERING  
SUBLIMATION PRODUCTS

by

Charles Acheamfour Baah

A THESIS

SUBMITTED TO THE FACULTY OF GRADUATE STUDIES  
IN PARTIAL FULFILLMENT OF THE REQUIREMENTS FOR THE  
DEGREE OF

MASTER OF SCIENCE

DEPARTMENT OF CHEMICAL AND PETROLEUM ENGINEERING

CALGARY, ALBERTA, CANADA

MAY, 1988

© CHARLES ACHEAMFOUR BAAH 1988

Permission has been granted to the National Library of Canada to microfilm this thesis and to lend or sell copies of the film.

The author (copyright owner) has reserved other publication rights, and neither the thesis nor extensive extracts from it may be printed or otherwise reproduced without his/her written permission.

L'autorisation a été accordée à la Bibliothèque nationale du Canada de microfilmer cette thèse et de prêter ou de vendre des exemplaires du film.

L'auteur (titulaire du droit d'auteur) se réserve les autres droits de publication; ni la thèse ni de longs extraits de celle-ci ne doivent être imprimés ou autrement reproduits sans son autorisation écrite.

ISBN 0-315-46554-9

THE UNIVERSITY OF CALGARY

FACULTY OF GRADUATE STUDIES

The undersigned certify that they have read, and recommend to the Faculty of Graduate Studies for acceptance, a thesis entitled,

"STUDIES IN RECOVERING SUBLIMATION PRODUCTS"

submitted by

Charles Acheamfour Baah in partial fulfillment of the requirements for the degree of Master of Science.

*M.A. Hastaoglu*

---

Dr. M.A. Hastaoglu, Committee Chairman  
Department of Chemical & Petroleum Engineering

*Franco Berruti*

---

Dr. F. Berruti  
Department of Chemical & Petroleum Engineering

*R.M. Butler*

---

Dr. R.M. Butler  
Department of Chemical & Petroleum Engineering

*K.L. Chowdhury*

---

Dr. K.L. Chowdhury  
Department of Mechanical Engineering

*24.05.1988*

---

Date

## ABSTRACT

A numerical model for recovering sublimation products, especially phthalic anhydride, is presented herein. Principles of mathematical modelling of finned tube desublimers and a procedure for solving the equations are discussed. The model permits a continuous determination of the phase change interface and the temperature distribution.

The model equations obtained are transformed into finite difference approximations and solved by an explicit method. Model predictions are compared to results obtained by mass transfer controlled desublimation.

The effects of the velocity and composition of the vapour-gas mixture, physical properties of the desubliming component, geometry of the fins, flow rate and properties of coolant are considered for the determination of the type of desublimation applicable. Key parameters are identified which affect the rate of desublimation of phthalic anhydride.

Model predictions are analyzed to assess the potential application of such methods to the recovery of sublimation products and desublimer design.

The important features of the model are:

- (i) Explicit formulation is used to prevent extensive storage,
- (ii) Exclusive use is made of two-dimensional formulation, and
- (iii) Curvature effects at the solid-gas interface are accounted for.

## ACKNOWLEDGEMENTS

I would like to express my sincere gratitude to Dr. M.A. Hastaoglu for initiating this project and for his continual support, encouragement and inspiration at every stage of this study.

I would also like to thank Mr. Paul Wellings and Ms. Isobel Vanstone of Academic Computing Services for their assistance in the computer program analysis.

My gratitude to Patricia Stuart-Bakes for her extraordinary social advice during some difficult periods, her excellent hospitality and sense of humour which made my stay in Canada a reality and for her precious golden time she spent on this thesis.

Finally, I would like to thank my wife to be, Julia Ivanovna Yurchak for her patience and tolerance.

I wish to dedicate this thesis to my wife to be, Julia Ivanovna Yurchak.

## TABLE OF CONTENTS

	Page No.
ABSTRACT	iii
ACKNOWLEDGEMENTS	v
TABLE OF CONTENTS	vi
LIST OF TABLES	viii
LIST OF FIGURES	ix
NOMENCLATURE	xii
1. INTRODUCTION	1
2. THEORETICAL ANALYSIS	8
2.1 Problem Formulation	8
2.2 Model Equations	8
2.2.1 Conservation Equations for Heat and Mass Flux	8
2.2.2 Numerical Solution Technique	16
3. CASE STUDIES	31
3.1 Physical Properties of Metal (including fins)	33
3.1.1 Effect of Thermal Diffusivities of Metals	33
3.1.2 Effect of Fin Height	37
3.1.3 Effect of Fin Height-to-pitch Ratio	39
3.2 Effect of Time on Development of the Deposition Profile	41
3.3 Effect of Coolant Properties	44
3.3.1 Effect of Inlet Temperature of Coolant	44

	Page
3.3.2 Effect of Type of Coolant	48
3.3.3 Effect of Flow Rate	52
3.4 Properties of Phthalic Anhydride	54
3.4.1 Effect of Thermal Properties of Phthalic Anhydride	54
3.5 Properties of Vapour-gas Mixture	56
3.5.1 Effect of Composition and Velocity of Vapour-gas Mixture	56
3.6 Temperature Profiles in the Coolant	60
3.7 Study of Isothermal Lines	60
3.8 Estimation of the Amount of Solid Formed	72
4. CONCLUSIONS AND RECOMMENDATIONS	75
4.1 Conclusions	75
4.2 Recommendations	76
REFERENCES	77

## LIST OF TABLES

Table No.	Title	Page No.
1	Comparison of Estimated Mass of Solid Formed for Different Tube Materials (including fins).	73
2	Comparison of Estimated Mass of Solid Formed for Different Flow Rates of Water, $T_c = 20^\circ\text{C}$ .	73
3	Comparison of Estimated Mass of Solid Formed for Different Coolants.	74

## LIST OF FIGURES

Figure No.	Title	Page No.
1	A Schematic diagram of a switch condenser.	9
2	Cross section of a finned tube showing direction of flow of coolant and vapour-gas mixture and formation of layers of phthalic anhydride.	10
3.	Grid point system showing a division of the system into seven regions.	18
4	Flow chart of the numerical algorithm.	27
5	Effect of thermal diffusivity of the metal on deposition, water as a coolant: $h = 20$ mm; $t = 16$ min.; $T_c = 20^\circ\text{C}$ .	36
6	Effect of fin height, water as a coolant: $p = 23$ mm; $T_c = 20^\circ\text{C}$ .	38
7	Effect of fin height-to-pitch ratio on the deposition profile: $h = 20$ mm; $t = 16$ min.; $T_c = 20^\circ\text{C}$ .	40
8	Deposition as a function of time, water as a coolant: $h = 20$ mm; $p = 19$ mm; $T_c = 10^\circ\text{C}$ .	42
9	Deposition as a function of time, water as a coolant: $h = 20$ mm; $p = 23$ mm; $T_c = 20^\circ\text{C}$ .	43
10	Effect of inlet temperature of ethylene glycol: $h = 20$ mm; $p = 23$ mm; $t = 16$ min.	45
11	Effect of inlet temperature of o-xylene on deposition: $h = 20$ mm; $t = 16$ min.	46
12	Effect of inlet temperature of water on deposition: $h = 20$ mm; $p = 23$ mm; $t = 16$ min.	47
13	Effect of coolant on deposition: $h = 20$ mm; $p = 23$ mm; $t = 16$ min.; $T_c = 10^\circ\text{C}$ .	49

Figure No.	Title	Page No.
14	Effect of coolant on deposition: $h = 20$ mm; $p = 23$ mm; $t = 16$ min.; $T_c = 20^\circ\text{C}$ .	50
15	Effect of coolant on deposition profile: $h = 20$ mm; $p = 23$ mm; $t = 16$ min.; $T_c = 40^\circ\text{C}$ .	51
16	Comparison of deposition of different flow rates: $h = 20$ mm; $p = 23$ mm; $t = 16$ min.; $T_c = 20^\circ\text{C}$ .	53
17	Effect of physical properties of solid on deposition: $h = 20$ mm; $p = 23$ mm; $t = 16$ min.; $T_c = 20^\circ\text{C}$ .	55
18	Effect of composition of vapour-gas mixture on deposition: $V_{vg} = 15$ m/s.	57
19	Effect of vapour-gas velocity on deposition: $X_{AO} = 0.09$ .	58
20	Temperature profiles of coolant (water): $h = 20$ mm; $p = 23$ mm; $t = 16$ min.; $T_c = 10^\circ\text{C}$ .	61
21	Temperature profiles of coolant (water): $h = 20$ mm; $p = 23$ mm; $t = 16$ min.; $T_c = 40^\circ\text{C}$ .	62
22	Plot of isothermal lines: $p = 23$ mm; $Q = 7.03 \times 10^{-5} \text{ m}^3/\text{s}$ ; $t = 16$ min.; $T_c = 20^\circ\text{C}$ .	65
23	Plot of isothermal lines: $p = 23$ mm; $Q = 3.02 \times 10^{-5} \text{ m}^3/\text{s}$ ; $t = 16$ min.; $T_c = 20^\circ\text{C}$ .	66
24	Plot of isothermal lines: $p = 19$ mm; $t = 16$ min.; $T_c = 10^\circ\text{C}$ .	67
25	Plot of isothermal lines: $p = 19$ mm; $t = 16$ min.; $T_c = 20^\circ\text{C}$ .	68

Figure No.	Title	Page No.
26	Plot of isothermal lines: $p = 23$ mm; $Q = 7.03 \times 10^{-5} \text{ m}^3/\text{s}$ ; $t = 16$ min.; $T_c = 10^\circ\text{C}$ .	69
27	Plot of isothermal lines, water as a coolant: $p = 23$ mm; $t = 16$ min.; $T_c = 40^\circ\text{C}$ .	70
28	Plot of isothermal lines, ethylene glycol as a coolant: $p = 23$ mm; $t = 16$ min.; $T_c = 40^\circ\text{C}$ .	71

## NOMENCLATURE

- $C_{AO}$  concentration of desubliming component in vapour-gas mixture,  $\text{kmol/m}^3$
- $C_{AS}$  concentration of desubliming component at the solid-gas interface,  $\text{kmol/m}^3$
- $c_s, c_L, c_m$  heat capacity of solid, coolant and metal respectively,  $\text{J/kg K}$
- $D_{ij}$  diffusion coefficient for a binary mixture,  $\text{cm}^2/\text{s}$
- $d_o$  outer diameter of the tube, m
- $\delta r$  interval between successive grid points in radial direction, m
- $\delta s$  dummy spatial interval, m
- $\delta t$  time increment, s
- $\delta z$  interval between successive grid points in axial direction, m
- $\Delta H$  latent heat of sublimation,  $\text{J/kg}$
- $\bar{h}_c$  heat transfer coefficient,  $\text{W/m}^2 \cdot \text{K}$
- $\bar{h}_{cm}$  heat transfer coefficient at coolant-metal interface,  $\text{W/m}^2 \cdot \text{K}$
- $h$  fin height, m
- $k$  Boltzmann's constant ( $5.735 \times 10^{-8} \text{ kW/m}^2 \cdot \text{K}^4$ )
- $k_i, k_j$  thermal conductivities of pure components
- $k_s, k_L, k_m$  thermal conductivity of solid, coolant and metal respectively,  $\text{W/m} \cdot \text{K}$
- $M$  molecular weight of desubliming component,  $\text{kg/kmol}$
- $M_i, M_j$  molecular weights of pure components,  $\text{kg/kmol}$

$N$  molar flux of desubliming component,  $\text{kmol/m}^2 \cdot \text{s}$   
 $n$  number of gaseous components  
 $p$  fin pitch, m  
 $P$  pressure, Pa  
PDE partial differential equation  
 $Q$  volumetric flow rate of coolant,  $\text{m}^3/\text{s}$   
 $R$  inner radius of tube, m  
 $r$  location of grid points in radial direction, m  
 $S_{ij}$  Sutherland constant for a binary mixture, K  
 $S_i, S_j$  Sutherland constants of pure components, K  
 $T$  temperature, K  
 $T_{\text{cm}}$  temperature at the coolant-metal interface,  $^{\circ}\text{C}$   
 $T_{\text{L}}$  temperature of coolant,  $^{\circ}\text{C}$   
 $T_{\infty}$  bulk temperature of vapour-gas mixture,  $^{\circ}\text{C}$   
 $T_{\text{b}}$  normal boiling point of a pure component, K  
 $T_{\text{c}}$  inlet temperature of coolant,  $^{\circ}\text{C}$   
 $t$  time, s  
 $U$  average velocity of coolant, m/s  
 $v$  volume of solid formed,  $\text{m}^3$   
 $V_{\text{vg}}$  velocity of vapour-gas mixture, m/s  
 $V_{\text{c}_i}, V_{\text{c}_j}$  critical molar volumes of pure components,  $\text{cm}^3/\text{g mole}$   
 $V_{\text{z}}$  velocity of coolant, m/s  
 $X_{\text{AO}}$  mole fraction of desubliming component in the vapour-gas mixture

$X_{AS}$  mole fraction of desubliming component at the solid-gas interface  
 $Y$  dummy solid thickness, m  
 $Y'$  rate of molar flux of the desubliming component, m/s  
 $y_i, y_j$  mole fractions of pure components  
 $Z$  length of tube, m

#### GREEK LETTERS

$\rho$  density,  $\text{kg/m}^3$   
 $\mu$  viscosity,  $\text{kg/m}\cdot\text{s}$   
 $\mu_i, \mu_j$  viscosities of pure components,  $\text{kg/m}\cdot\text{s}$   
 $\alpha$  thermal diffusivity,  $\text{m}^2/\text{s}$   
 $\alpha_s, \alpha_L, \alpha_m$  thermal diffusivity of solid, coolant and metal respectively,  $\text{m}^2/\text{s}$   
 $\lambda$  dummy spatial interval, m  
 $\epsilon$  collision integral  
 $\sigma$  collision diameter, m

#### SUBSCRIPTS

$l$  coolant  
 $m$  metal  
 $o$  initial value  
 $s$  solid

des desublimation

vg vapour-gas

#### **SUPERSCRIPTS**

n previous time level

n+1 present time level

## CHAPTER 1

### INTRODUCTION

In many chemical engineering processes, especially in vapour phase catalytic oxidation of hydrocarbons with atmospheric oxygen, vapour-gas mixtures are obtained that contain 0.2 - 1.5 vol.% of the target product. The second step in the manufacture of most organic sublimation products is the separation of the target product from the vapour-gas mixture leaving the reactor. Such products are separated by desublimation resulting from contact of the vapour-gas mixture with a cooling finned tube surface. Due to the cold metal surface, the desublimated deposits on the tubes, heat is then applied and the intermediate product is melted and collected. Fins serve to extend the heat-transfer surface of the tube and the rate of heat transfer through the tube wall. The increase in heat flow is approximately proportional to the amount of fin surface added. Flexibility in both material and design configurations allows finned tubing to be used in a variety of applications. The mathematical modelling of these systems could be important for desublimator design. This is a moving boundary problem since the position of the phase boundary (solid-gas interface) changes with the progress of the operation.

Despite the importance of the topic, a literature search revealed relatively few solutions which may be extended to practical problems.

Analytical solutions are limited due to the mathematical complexity and complicated boundary conditions, while numerical solutions have not been developed. Numerical methods of solution are useful for such situations. Desublimation of organic compounds is a problem of considerable practical and theoretical importance. The practical importance of this problem is provided by the fact that desublimation of organic compounds allows the recovery of sublimation products from vapour-gas mixtures. The theoretical significance of these problems is associated with the fact that while some experimental and analytical work has been done on the recovery of sublimation products in tubular systems, numerical modelling for recovering sublimation products on straight finned tubes has received no attention up to the present. Thus the construction of finned tube desublimers is hindered by the lack of numerical models.

An extensive literature survey shows that relatively little work has been done in the area of desublimation of organic products, especially on desublimation of phthalic anhydride and maleic anhydride in tubular apparatus and nothing has been done on desublimation of organic products on cooled, straight finned tubes. This is surprising since finned surfaces are widely known for their use as good heat exchangers for numerous chemical process operations.

Originally a series of either air or water-cooled chambers were used - for example, by Badische Anilin-und Soda-Fabrik A.-G. (BASF) in

Germany (1896) in the manufacture of phthalic anhydride from the vapour-gas mixture. Another process used the washing of the phthalic anhydride from the reactor vapour-gas mixture with water, but the subsequent removal of the water was difficult and created a waste disposal problem.

A work on separating phthalic anhydride from reaction gases on finned tube bundles bent into a hairpin shape was patented by Wagner et al. (BASF, A-G) (1974). Different authors started to develop simple methods of separating the phthalic anhydride from the vapour-gas mixture.

Sapozhnikov (1974) used a gas-dust heat transfer agent in the manufacture of phthalic anhydride but no details of his work were given.

Krupiczka and Bilik (1980) performed an experiment on heat transfer during desublimation of phthalic anhydride but there is no literature on their work either. Later on, they developed a model to consider the simultaneous heat and mass transfer in the gas phase. An experimental work was also carried out but no details were given on the type of apparatus used.

None of the authors above studied the factors and key parameters which affect desublimation.

The effect of the composition of the target product in the vapour-gas mixture is important for the determination of the type of desublimation applicable. The influence of the composition of phthalic anhydride in the vapour-gas mixture on the rate of desublimation was studied by Gevorkyan et al. (1980). They found experimentally that an increase in the mole fraction of phthalic anhydride in the vapour-gas mixture increases the yield of desublimed product. It was also demonstrated that mass transfer controlled desublimation was more than twice as efficient under turbulent rather than laminar-flow conditions, but details of the type of apparatus used for their study were not given.

Gorelik et al. (1980) developed a mathematical model for desublimation of organic products, especially phthalic anhydride and maleic anhydride, in a tubular system. They applied an analytical technique to solve the model equations. Experiments were also performed in order to compare the experimental results with the model predictions. The main disadvantage of their work was that the tubes easily got choked. To prevent this in all cases, the vapour-gas mixture was warmed up.

Korobchanskii et al. (1981) developed a condenser for increasing the heat transfer and decreasing the losses during phthalic anhydride recovery from naphthalene oxidation product. In their work, descending cold metal spheres contact the ascending vapour-gas mixture and phthalic anhydride desublimes on the spheres. The latter are passed

into a melting zone where the product is removed. The metal spheres are withdrawn, cooled and recycled.

None of the work of these authors described above studied the temperature profile in the solid. It is, therefore, clear that no work has been done on desublimation of organic products on straight finned tubes and, to the author's knowledge, no numerical technique has been applied to solve this problem.

Phase change problems where the position of the phase boundary in general is not known are of the moving boundary type. For a variety of these problems, there are solutions available in the literature. The solutions in general differ according to the boundary conditions, co-ordinate dimensions and solution technique. (See Ockendon and Hodkins (1975), Lewis and Morgan (1979), Epstein and Cheung (1983) and Cheung and Epstein (1984) for a large number of references.)

Otis (1956), Neel (1952) and Von Glahn (1955) have developed analog circuits for studying simple problems involving melting of solids and Goodman (1958) developed an approximate technique for determining the position of a melting front.

Forster (1954) extended the conventional complete difference equations for fixed network spacing to solve a phase change problem. The fusion front travel was computed continuously by using a quadratic

through the interface and at two adjoining points to obtain the slope of the temperature at the fusion point.

Voller and Cross (1983) used an explicit numerical method to track a moving phase change front. Pham (1985) applied a fast unconditionally stable finite-difference scheme to solve a heat conduction problem with phase change. None of the above mentioned methods can be applied directly to desublimation of organic products on finned tubes because of the complexity of the system. This means, of course, that there is no numerical model which is general enough to study the factors which affect both the deposition and temperature profiles. In this thesis, a two-dimensional desublimation of phthalic anhydride is solved through numerical methods using a grid system developed by Murray and Landis (1959), extended to two dimensions by Springer and Olson (1961) and later on applied by Hastaoglu (1986) and (1987).

The aim of this work was, therefore, to develop a numerical model for recovering sublimation products on finned tube bundles in a switch condenser and to study the key parameters which affect the deposition rate and temperature profiles. The system selected for the study is the recovery of phthalic anhydride on straight finned tubes. The effect of the growth of phthalic anhydride crystals on the deposition profile or rate of desublimation was not considered.

Equations describing the conservation of energy are partial differential equations. The equation governing the movement of the phase boundary (solid-gas interface) is an ordinary differential equation. Due to the complexity of the model equations, a numerical solution was utilized. Space and time derivatives were approximated by finite differences to obtain a numerical model. Model predictions were generated for some different test cases.

As far as the organization of this thesis is concerned, the mathematical formulation of the problem and numerical solution technique are outlined in Chapter 2. Chapter 3 deals with case studies, analysis and discussion of results. Concluding remarks and recommendations for future studies are given in Chapter 4.

## CHAPTER 2

### THEORETICAL ANALYSIS

#### 2.1 Problem Formulation:

A schematic diagram of a switch condenser is shown in Figure 1. The unit consists of the following:

- (i) outer shell
- (ii) finned tubes.

Consider a straight finned tube through which a coolant is flowing and across it flows a vapour-gas mixture. When the temperature of the metal surface is lower than the desublimation temperature of the component in the gas to be removed, there is a phase change at the interface between the metal and the vapour-gas mixture. Phthalic anhydride solidifies on the cool finned surface. (See Figure 2).

The desubliming component is transferred to the cold surface from the vapour-gas mixture and deposited on the tubes via mass transfer. There is heat transfer in the gas phase as well as in the solid phase.

#### 2.2 Model Equations

##### 2.2.1 Conservation equations for heat and mass fluxes

The conservation of heat can be written in various regions as:

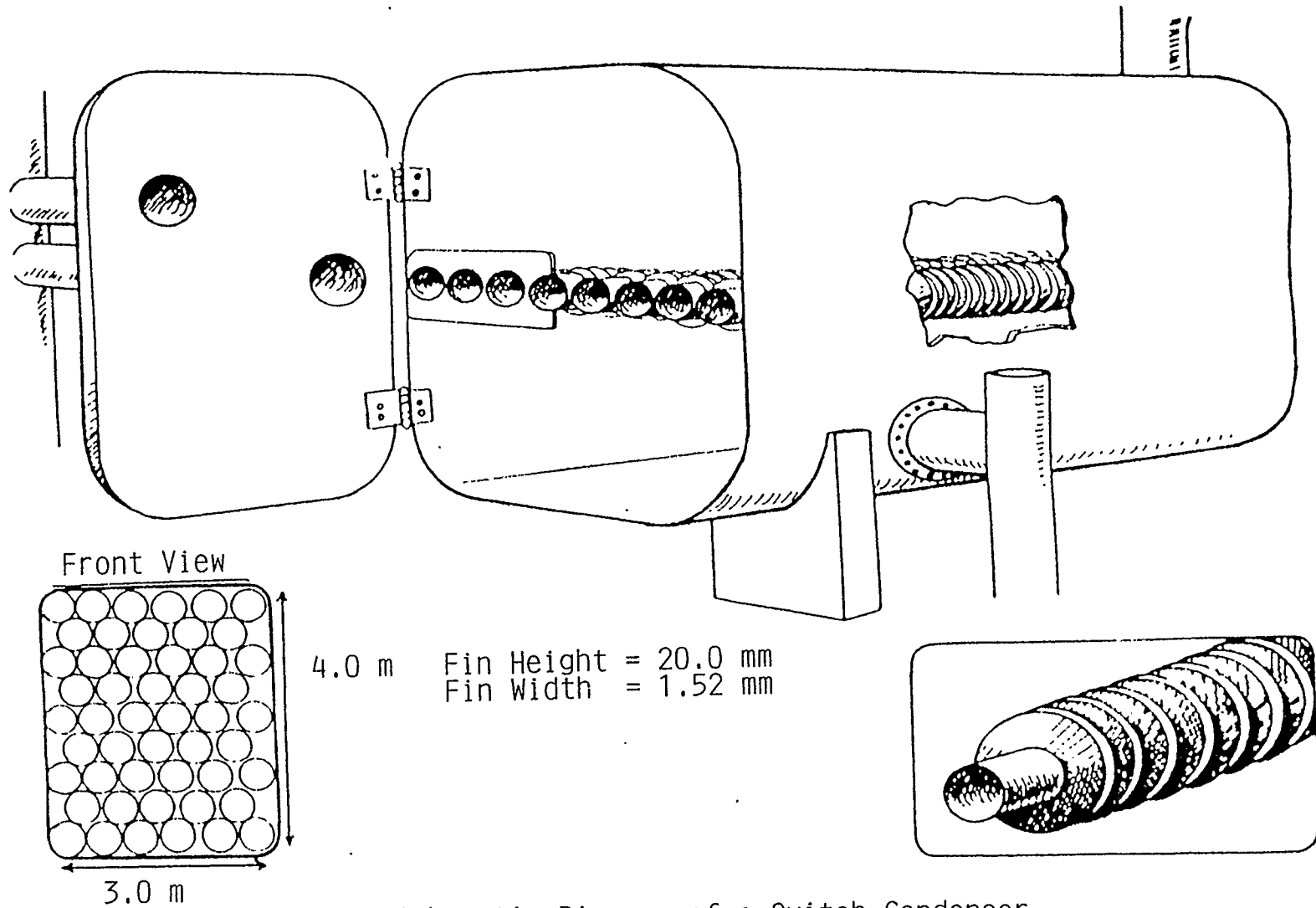


FIGURE 1: A Schematic Diagram of a Switch Condenser

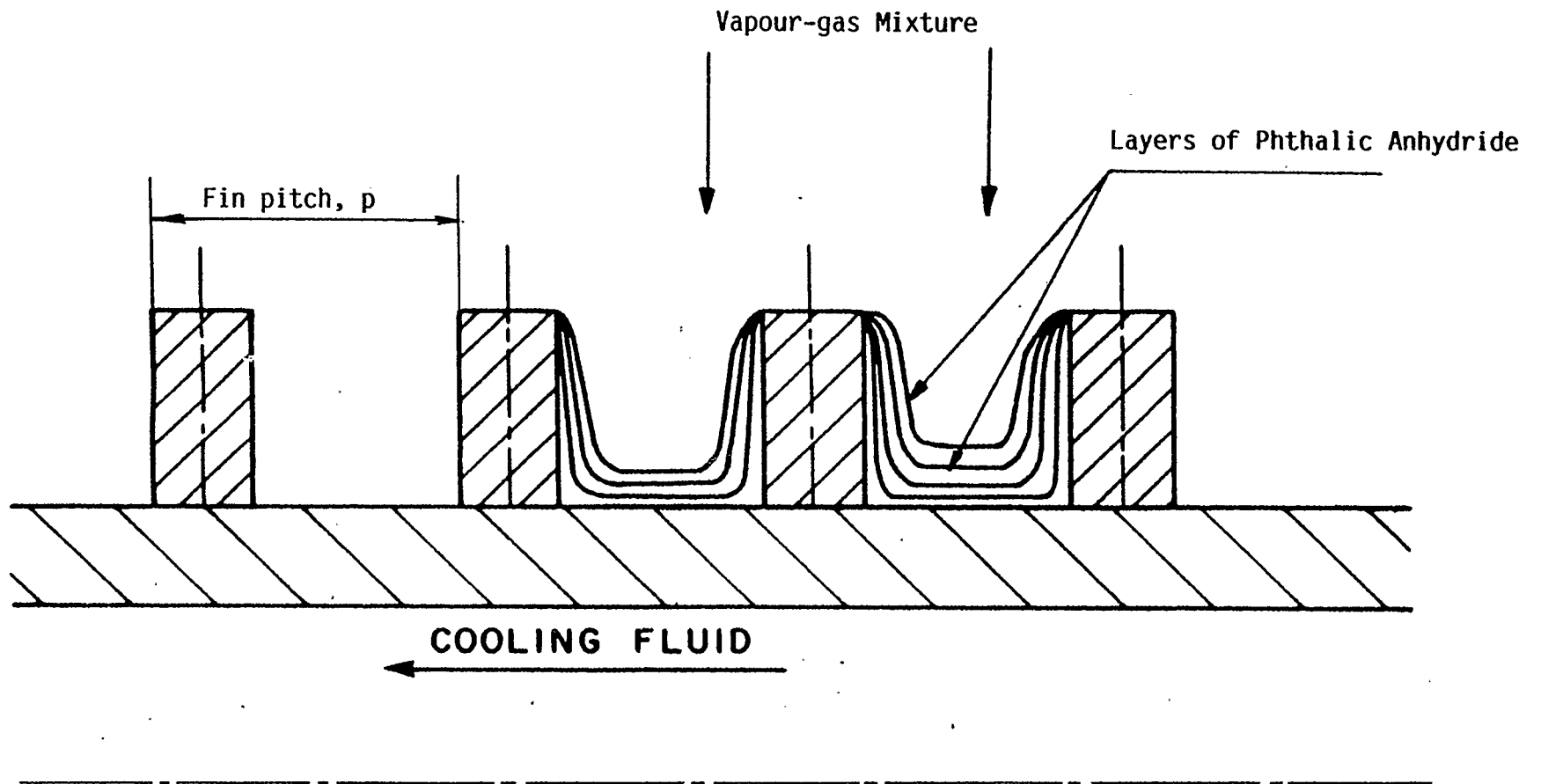


FIGURE 2. Cross Section of a Finned Tube Showing Direction of Flow of Coolant and Vapour-Gas Mixture and Formation of Layers of Phthalic Anhydride.

**Coolant:**

The energy equation in cylindrical coordinates, assuming radial symmetry, is given by,

$$\rho_L C_L \left( \frac{\partial T}{\partial t} + v_z \frac{\partial T}{\partial z} \right) = k_L \left[ \frac{1}{r} \frac{\partial}{\partial r} \left( r \frac{\partial T}{\partial r} \right) + \frac{\partial^2 T}{\partial z^2} \right]. \quad (1)$$

Assuming a parabolic velocity profile, the momentum and continuity equations are satisfied by,

$$v_z = 2U \left[ 1 - \left( \frac{r}{R} \right)^2 \right]. \quad (2)$$

Combining equations (1) and (2), the required energy equation for the coolant is,

$$\rho_L C_L \left[ \frac{\partial T}{\partial t} + 2U \left( 1 - \left( \frac{r}{R} \right)^2 \right) \frac{\partial T}{\partial z} \right] = k_L \left[ \frac{1}{r} \frac{\partial}{\partial r} \left( r \frac{\partial T}{\partial r} \right) + \frac{\partial^2 T}{\partial z^2} \right]. \quad (3)$$

Equation (3) is undefined at  $r = 0$  (centre of the tube). The discontinuity can be eliminated by evaluating the limiting form of the first term on the right hand side using L'Hopital's rule as follows:

$$\left( \frac{1}{r} \frac{\partial T}{\partial r} \right) \approx \frac{\partial^2 T}{\partial r^2} \Big|_{(\text{near axis})}. \quad (4)$$

The energy equation applicable at the centre of the tube is therefore,

$$\rho_L C_L \left( \frac{\partial T}{\partial t} + 2U \frac{\partial T}{\partial z} \right) = k_L \left[ 2 \frac{\partial^2 T}{\partial r^2} + \frac{\partial^2 T}{\partial z^2} \right]. \quad (5)$$

Where there is laminar flow, one should use grid points in the coolant. In all other cases the equation in the coolant can be ignored and a heat transfer coefficient at the coolant-metal interface has to be used. The flux boundary condition is given below.

$$k_m \frac{\partial T}{\partial r} \Big|_{\text{wall}} = \bar{h}_{\text{cm}} (T_{\text{cm}} - T_L) \quad (5a)$$

The conservation of heat in the metal and solid can also be written as follows:

Metal:

$$\rho_m C_m \frac{\partial T}{\partial t} = k_m \left[ \frac{1}{r} \frac{\partial}{\partial r} \left( r \frac{\partial T}{\partial r} \right) + \frac{\partial^2 T}{\partial z^2} \right]. \quad (6)$$

Solid:

$$\rho_s C_s \frac{\partial T}{\partial t} = k_s \left[ \frac{1}{r} \frac{\partial}{\partial r} \left( r \frac{\partial T}{\partial r} \right) + \frac{\partial^2 T}{\partial z^2} \right]. \quad (7)$$

The energy equation at the coolant-metal interface is obtained by observing that the heat flux must be continuous so that,

$$k_L \frac{\partial T}{\partial r} = k_m \frac{\partial T}{\partial r} . \quad (8)$$

Similarly, at the metal-solid interface,

$$k_m \frac{\partial T}{\partial r} = k_s \frac{\partial T}{\partial r} \quad (9)$$

and

$$k_m \frac{\partial T}{\partial z} = k_s \frac{\partial T}{\partial z} . \quad (10)$$

For a two-dimensional problem in a cylindrical coordinate system involving  $(r, z, t)$  the interface equation (if supercooling is ignored) takes the form,

$$\rho_s \Delta H \frac{dY}{dt} = \left[ 1 + \left( \frac{\partial Y}{\partial z} \right)^2 \right] \left[ k_s \frac{\partial T}{\partial r} - \bar{h}_c \left( T_{des} - T_\infty \right) \right] \quad (11)$$

where  $Y$  is the location of the solid-gas interface from the surface of the tube.

The term on the left hand side represents the movement of the phase front upon desublimation. The factor in brackets on the right hand side accounts for curvature effects. The second factor represents the net amount of heat transfer into the solid.

The heat transfer on the vapour-gas mixture side is controlled by convection characterized by a heat transfer coefficient,  $\bar{h}_c$ , rather than conduction because of the movement of the gas phase at a certain

velocity towards the finned structure.

Equation (11) is used when the deposition profile is developed. When the profile is not developed (at the beginning), equation (11) would collapse at surfaces perpendicular to the z-direction. Therefore, the problem can be considered as one-dimensional on the surface and the applicable equation can be written as,

$$\rho_s \Delta H \frac{dY}{dt} = k_s \frac{\partial T}{\partial r} - \bar{h}_c \left( T_{des} - T_\infty \right) \quad (12)$$

or

$$\rho_s \Delta H \frac{dY}{dt} = k_s \frac{\partial T}{\partial z} - \bar{h}_c \left( T_{des} - T_\infty \right) . \quad (13)$$

depending on which direction the computation is being made.

In desublimation, the phase change would occur due to heat transfer but the desubliming component has to be transferred via mass transfer to the solid-gas interface. Therefore, it is imperative to compare these two rates. The phase change rate due to mass transfer can be obtained using an F-type mass transfer coefficient (see Treybal, 1980) as follows:

$$N = F \ln \frac{1 - X_{AS}}{1 - X_{AO}} . \quad (14)$$

The interface mole fraction,  $X_{AS}$  is calculated from the interface concentration  $C_{AS}$ , which is determined from the vapour pressure - temperature relation for phthalic anhydride and the perfect gas law.

The necessary initial and boundary conditions which can easily be modified for other situations, are as follows:

Initial conditions:

$$\text{coolant: } T_c = T_{co} \quad \text{at } 0 \leq r \leq R \quad 0 \leq z \leq Z \quad t = 0. \quad (15)$$

$$\text{metal: } T_m = T_{mo} \quad \text{at } t = 0. \quad (16)$$

$$\text{solid: } Y = 0 \quad (\text{There is no solid initially}). \quad (17)$$

Boundary Conditions:

$$T_c = T_{co} \quad \text{at } z = 0, \quad t > 0, \quad (18)$$

$$k_L \frac{\partial T}{\partial r} = k_m \frac{\partial T}{\partial r} \quad \text{at } r = R, \quad t > 0, \quad (19)$$

$$T_{vg} = T_{des}, \quad C_A = C_{AS} \quad \text{at the solid-gas interface, } t > 0. \quad (20)$$

The assumptions implicit in the model equations are:

- i) The physical properties of the coolant, metal and solid are independent of temperature and position.
- ii) The heat transfer coefficient is uniform over the entire fin surface.
- iii) Good contact exists between fins and tube and contact resistance between the fins and tube is neglected.
- iv) The coolant velocity profile is not affected by temperature.
- v) The solid-gas interface is smooth.
- vi) There is a single phase temperature at the interface.

Equations with initial and boundary conditions (eqs. 3, 5-11) have

to be solved simultaneously. Due to the complexity of these equations, it is impossible to solve them analytically. Therefore, a numerical procedure is used. The following section describes the technique used.

### 2.2.2 Numerical Solution Technique.

The standard procedure in the numerical method used is to decide on the number of grid points to be used in each region and then to write down the system equations in finite difference form using new time step values and previous time step values. For this purpose, an implicit, explicit or Crank-Nicolson type approach can be used.

Because of the shape of the system, generally, a large number of nodes are required to cover the whole system.

Implicit methods are less restrictive to the size of the time step. The advantage of the implicit method over the explicit one is that the former is stable for all sizes of time step; thus, there is no size restriction on  $dt$ . The only size restriction on  $dt$  is due to the consideration of the truncation error.

Because of the nature of the boundary conditions and the number of grid points required, it is extremely difficult to apply an implicit method to this system. It would require tremendous computer storage. Because of this, an explicit method is used in this thesis.

To apply the explicit method, the model is broken down into the following regions:

- I Flowing coolant in the tubes,
- II Boundary between coolant and metal,
- III Metal, including fins,
- IV Boundary between metal and solid,
- V Solid,
- VI Horizontal boundary between solid and vapour-gas mixture,
- VII Vertical boundary between solid and vapour-gas mixture.

These regions are shown in Figure 3. The temperature profile in each region is solved by a different partial differential equation (PDE).

Each region (coolant, metal) is divided into a fixed number of grid points. Grid points are introduced in the solid as the latter is being formed. The solution is obtained at regularly spaced intervals of  $\delta r$  and  $\delta z$  which are found from the number of grid points in the radial and axial directions respectively. The location of the  $i$  th grid point (in the radial direction) is obtained from the following equation:

$$r_i = (i-1) \delta r \quad (21)$$

where  $\delta r$  is related to the number of grid points,  $nr$ , and the radius of the tube as

$$\delta r = \frac{R}{nr-1} \quad (22)$$

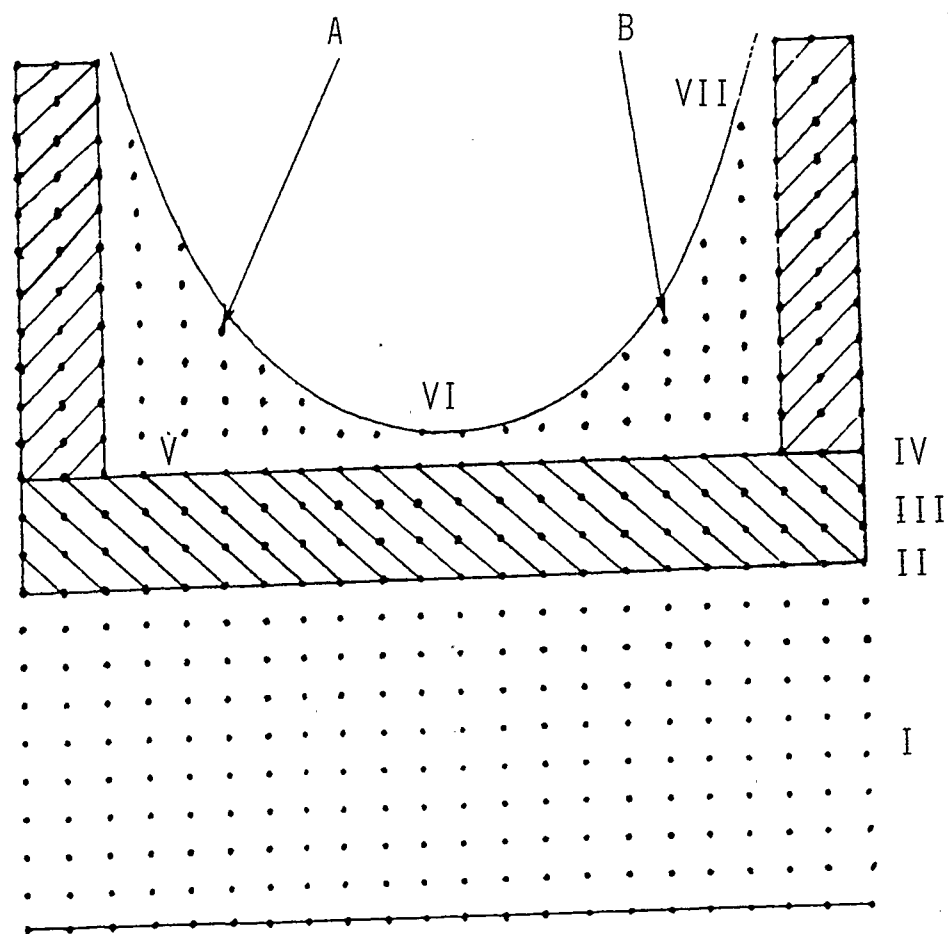


FIGURE 3: Grid Point System Showing a Division of the System into Seven Regions.

Similarly, for the location of the  $j$  th grid point (in the axial direction),

$$z_j = j \cdot \delta z \quad (23)$$

where  $\delta z$  is related to  $nz$ , the number of grid points along the length of the tube.

The model equations are discretized by finite-difference approximations. The temporal derivative is discretized as:

$$\frac{\partial T}{\partial t} \approx \frac{T_{i,j}^{n+1} - T_{i,j}^n}{\delta t} \quad (24)$$

To illustrate the salient features of the numerical technique, the discretization of equations (3,5-7,11) are shown below. For cylindrical geometry, the expansion of the Laplacian operator yields the following equations:

Coolant (excluding grid points at the centre of the tube):

$$\begin{aligned} T_{i,j}^{n+1} = & T_{i,j}^n + \alpha_L \cdot \delta t \left[ \left( T_{i-1,j}^n - 2T_{i,j}^n + T_{i+1,j}^n \right) \cdot \frac{1}{(\delta r)^2} \right. \\ & + \frac{1}{2(i-1)(\delta r)^2} \left( T_{i+1,j}^n - T_{i-1,j}^n \right) + \frac{1}{(\delta z)^2} \left( T_{i,j-1}^n - 2T_{i,j}^n \right. \\ & \left. \left. + T_{i,j+1}^n \right) \right] - 2U \left[ 1 - \left( \frac{(i-1)}{R} \right)^2 \right] \left[ \frac{1}{2\delta z} \left( T_{i,j+1}^n - T_{i,j-1}^n \right) \right] \end{aligned} \quad (25)$$

The equation for grid points at the centre of the tube is given as follows:

$$\begin{aligned}
 T_{i,j}^{n+1} = & T_{i,j}^n + \alpha_L \cdot \delta t \left[ \frac{2}{(\delta r)^2} \left( T_{i-1,j}^n - 2T_{i,j}^n + T_{i+1,j}^n \right) \right. \\
 & \left. + \frac{1}{(\delta z)^2} \left( T_{i,j-1}^n - 2T_{i,j}^n + T_{i,j+1}^n \right) \right] - \frac{U}{\delta z} \left( T_{i,j+1}^n - T_{i,j-1}^n \right)
 \end{aligned} \tag{26}$$

The discretization of equations (6) and (7) proceeds similarly.

The resulting equations are shown below:

$$\begin{aligned}
 T_{i,j}^{n+1} = & T_{i,j}^n + \alpha_m \cdot \delta t \left[ \left( T_{i-1,j}^n - 2T_{i,j}^n + T_{i+1,j}^n \right) \cdot \frac{1}{(\delta r)^2} \right. \\
 & \left. + \frac{1}{2(i-1)(\delta r)^2} \left( T_{i+1,j}^n - T_{i-1,j}^n \right) + \frac{1}{(\delta z)^2} \left( T_{i,j-1}^n - 2T_{i,j}^n + T_{i,j+1}^n \right) \right]
 \end{aligned} \tag{27}$$

$$\begin{aligned}
 T_{i,j}^{n+1} = & T_{i,j}^n + \alpha_s \cdot \delta t \left[ \left( T_{i-1,j}^n - 2T_{i,j}^n + T_{i+1,j}^n \right) \cdot \frac{1}{(\delta r)^2} \right. \\
 & \left. + \frac{1}{2(i-1)(\delta r)^2} \left( T_{i+1,j}^n - T_{i-1,j}^n \right) + \frac{1}{(\delta z)^2} \left( T_{i,j-1}^n - 2T_{i,j}^n + T_{i,j+1}^n \right) \right]
 \end{aligned} \tag{28}$$

The equation for grid points next to the solid-gas interface is obtained by taking into account the curved boundaries. (See grid points A and B in Figure 3). When a region has a curved boundary, it

is possible that the curved boundary intersects the finite-difference network at points that are not the grid points. Then the finite difference formulae derived for the other grid points are not applicable to represent the derivatives at a grid point near the solid-gas interface. The temperature of such points are calculated by the equation below

$$\begin{aligned}
T_{i,j}^{n+1} = & T_{i,j}^n + \alpha_s \cdot \delta t \left[ \frac{1}{(\delta z)^2} \left( T_{i,j-1}^n - 2T_{i,j}^n + T_{i,j+1}^n \right) \right. \\
& + \frac{1}{2(i-1)(\delta r)^2} \left( \frac{T_{des}}{\lambda(1+\lambda)} - \frac{\lambda}{1+\lambda} T_{i-1,j}^n + \frac{(\lambda-1)}{\lambda} T_{i,j}^n \right) \\
& \left. + \frac{2}{(\delta r)^2} \left( \frac{T_{des}}{\lambda(1+\lambda)} + \frac{T_{i-1,j}^n}{1+\lambda} - \frac{T_{i,j}^n}{\lambda} \right) \right] \quad (29)
\end{aligned}$$

The discretization of equation (8) is derived by applying finite difference approximations at the interface between two different media (coolant and metal). The discretized equation for the computation of new temperatures at the coolant-metal interface is given as follows:

$$T_{i,j}^{n+1} = \frac{1}{\frac{\rho_L C_L}{2\delta r + \frac{1}{(i-1)\delta r}} - \frac{\rho_m C_m}{\frac{1}{(i-1)\delta r} - \frac{2}{\delta r}}} \left\{ \frac{k_L}{\delta r + \frac{1}{(i-1)\delta r}} \left[ \frac{T_{i,j}^n}{\alpha_L} + \frac{2\delta t}{(\delta r)^2} \right] \right.$$

$$\begin{aligned}
& \left[ T_{i-1,j}^n - T_{i,j}^n \right] + \frac{\delta t}{(\delta z)^2} \left[ T_{i,j+1}^n - 2T_{i,j+1}^n + T_{i,j-1}^n \right] + \frac{k_m}{\frac{1}{(i-1)\delta r} - \frac{2}{\delta r}} \\
& \left[ -\frac{T_{i,j}^n}{\alpha_m} - \frac{2\delta t}{(\delta r)^2} \left[ T_{i+1,j}^n - T_{i,j}^n \right] - \frac{\delta t}{(\delta z)^2} \left[ T_{i,j+1}^n - 2T_{i,j}^n + T_{i,j-1}^n \right] \right] \Bigg\} \\
& \tag{30}
\end{aligned}$$

The discretization of equations (9) and (10) can be obtained similarly. The resulting equations are shown below.

$$\begin{aligned}
T_{i,j}^{n+1} &= \frac{1}{\frac{\rho_m C_m}{\frac{2}{\delta r} + \frac{1}{(i-1)\delta r}} - \frac{\rho_s C_s}{\frac{1}{(i-1)\delta r} - \frac{2}{\delta r}}} \left\{ \frac{k_m}{\frac{2}{\delta r} + \frac{1}{(i-1)\delta r}} \left[ \frac{T_{i,j}^n}{\alpha_m} + \frac{2\delta t}{(\delta r)^2} \right. \right. \\
& \left. \left[ T_{i-1,j}^n - T_{i,j}^n \right] + \frac{\delta t}{(\delta z)^2} \left[ T_{i,j+1}^n - 2T_{i,j+1}^n + T_{i,j-1}^n \right] + \frac{k_s}{\frac{1}{(i-1)\delta r} - \frac{2}{\delta r}} \right. \\
& \left. \left. \left[ -\frac{T_{i,j}^n}{\alpha_m} - \frac{2\delta t}{(\delta r)^2} \left[ T_{i+1,j}^n - T_{i,j}^n \right] - \frac{\delta t}{(\delta z)^2} \left[ T_{i,j+1}^n - 2T_{i,j}^n + T_{i,j-1}^n \right] \right] \right\} \\
& \tag{31}
\end{aligned}$$

$$\begin{aligned}
T_{i,j}^{n+1} &= \frac{1}{\rho_m C_m + \rho_s C_s} \left\{ k_s \left[ -\frac{T_{i,j}^n}{\alpha_s} + \frac{\delta t}{2(i-1)(\delta r)^2} \left[ T_{i+1,j}^n - T_{i-1,j}^n \right] \right. \right. \\
& \left. \left. + \frac{\delta t}{(\delta r)^2} \left[ T_{i+1,j}^n - 2T_{i,j}^n + T_{i-1,j}^n \right] + \frac{2\delta t}{(\delta z)^2} \left[ T_{i,j+1}^n - T_{i,j}^n \right] \right] \right\}
\end{aligned}$$

$$\begin{aligned}
& + k_m \left[ \frac{T_{i,j}^n}{\alpha_m} + \frac{2\delta t}{(\delta z)^2} \left( T_{i,j-1}^n - T_{i,j}^n \right) + \frac{\delta t}{2(i-1)(\delta r)^2} \left( T_{i+1,j}^n - T_{i-1,j}^n \right) \right. \\
& \quad \left. + \frac{\delta t}{\delta r^2} \left( T_{i+1,j}^n - 2T_{i,j}^n + T_{i-1,j}^n \right) \right] \Bigg\}. \tag{32}
\end{aligned}$$

The explicit form of finite difference representation given by the above equations (25 - 32) provides a relatively straight forward expression for the determination of the unknown  $T_{i,j}^{n+1}$  at a new time step, from the knowledge of  $T_{i,j}^n$ , at the previous time step.

Equation (11) which describes the movement of the solid-gas interface is derived from the normal interface condition (see Ozisik (1980)). This can be written in discretized form as:

$$\begin{aligned}
Y_{i,j}^{n+1} &= Y_{i,j}^n + \frac{\delta t}{\rho_s \cdot \Delta H} \left[ \frac{k_s}{d_{s,i,j}} \left( T_{des} - T_{i,j}^n \right) - \bar{h}_c \left( T_{des} - T_\infty \right) \right] \\
& \quad \left[ 1 + \left( \frac{Y_{i,j+1}^n - Y_{i,j-1}^n}{2\delta z} \right)^2 \right] \tag{33}
\end{aligned}$$

where the last term in the last brackets accounts for the curvature effect at the solid-gas interface. Equation (33) only applies when the deposition profile is developed, otherwise the terms which account for the curvature effect are omitted, i.e., the problem is considered as one-dimensional and the equation is given as follows:

$$Y_{i,j}^{n+1} = Y_{i,j}^n + \frac{\delta t}{\rho_s \Delta H} \left[ k_s \frac{T_{des} - T_{i,j}^n}{d_{s_{i,j}}} - \bar{h}_c (T_{des} - T_\infty) \right] \quad (34)$$

where  $d_{s_{i,j}}$  is the spatial step size in the direction of interest.

At the early stages of the computation of the movement of the solid-gas interface, because of limited amount of solid phthalic anhydride on the tube,  $k_s \frac{\partial T}{\partial r}$  in equation (12) and  $k_s \frac{\partial T}{\partial z}$  in equation (13) are calculated by the approximations given below

$$k_s \frac{\partial T}{\partial z} \approx \frac{T_{des} - T_{i,j-1}}{\frac{Y_j}{k_s} + \frac{\delta z}{k_m}} \quad (35)$$

and

$$k_s \frac{\partial T}{\partial r} \approx \frac{T_{des} - T_{i-1,j}}{\frac{Y_i}{k_s} + \frac{\delta r}{k_m}} \quad (36)$$

This is necessary because the amount of solid formed is not enough to use the discretized form of  $\frac{\partial T}{\partial z}$  and  $\frac{\partial T}{\partial r}$ . Their discretized forms are applied immediately after solid is formed to allow some grid points in the solid. This technique allows the model to be stable for any initial thickness of solid used to begin the computations.

#### Stability of the Method.

Stability is affected by the time step chosen. However, the error between the numerical and actual solution increases as  $\delta r$  or  $\delta z$

increases, which is an added consideration in the selection of  $\delta r$  and  $\delta z$ .

The time step is chosen to satisfy the following conditions:

$$\delta t \leq \left( \frac{(\delta z)^2}{2\alpha_L} \right) ; \quad \delta t \leq \left( \frac{(\delta z)^2}{2\alpha_s} \right) ; \quad \delta t \leq \left( \frac{(\delta z)^2}{2\alpha_m} \right) ; \quad (37a)$$

$$\delta t \leq \left( \frac{(\delta r)^2}{2\alpha_L} \right) ; \quad \delta t \leq \left( \frac{(\delta r)^2}{2\alpha_s} \right) ; \quad \delta t \leq \left( \frac{(\delta r)^2}{2\alpha_m} \right) . \quad (37b)$$

#### Solution Procedure:

The energy equation for each region is solved separately. The temperatures of grid points at the centre of the tube are first evaluated using equation (26). Equation (27) is then used to evaluate temperatures of grid points in the other parts of the coolant. Once these temperatures are evaluated, equation (30) is used to evaluate the temperatures of grid points at the coolant-metal interface. The temperatures of grid points in the metal (including fins) are then evaluated using equation (27). Equations (31) and (32) are then used to evaluate the temperatures of grid points at the metal-solid interface. Equation (28) is used to evaluate the temperatures of grid points in the solid (excluding those next to the solid-gas interface). Equation (29) is then used to evaluate the temperatures of grid points next to the solid-gas interface. The movement of the solid-gas interface is then determined using equation (33). This procedure is necessary because of the division of the system.

The flow chart of the numerical algorithm is presented in Figure 4. The time is advanced by one time step and the new temperature profiles and solid-gas interface are determined for the new time. If the location of the solid-gas interface (thickness of solid formed) is less than the height of the fin, the temperatures and thickness are updated for the new time. The process will continue until the fins have been filled or until the resistance to heat transfer through the metal and solid formed cannot be overcome by the coolant.

The equations used for the calculation of the molecular diffusivity, viscosity of the vapour-gas mixture, thermal conductivity of the vapour-gas mixture and heat and mass transfer coefficients are presented in the following section.

i. Heat and mass transfer coefficients,  $\bar{h}_c$  and F.

Heat and mass transfer are described based on overall coefficients calculated from empirical correlations. Their magnitudes are dependent on the geometry of the system, velocity and physical properties of the vapour-gas mixture.

The external heat and mass transfer coefficients are calculated from well established correlations. For flow of a fluid at right angles to a circular cylinder with a Reynolds number in the range of  $0.1 - 10^5$  and a Schmidt number in the range of  $0.7 - 1500$ , McAdams (1954) proposed the following correlation:

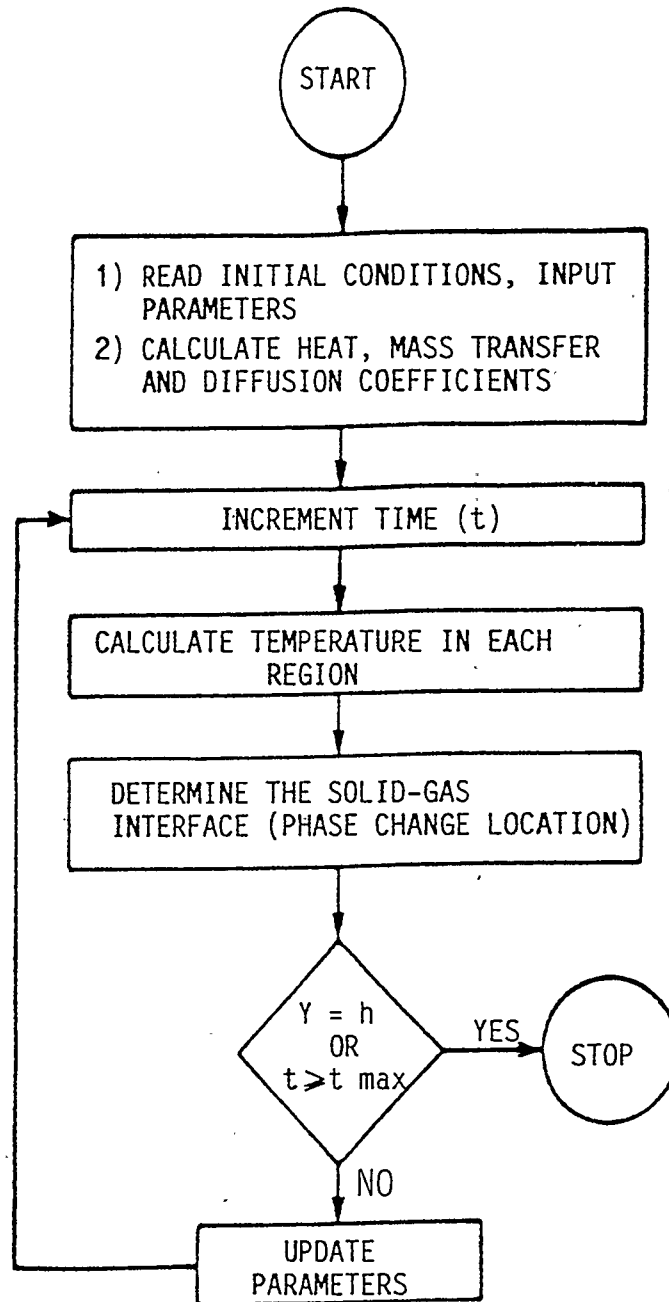


FIGURE 4: Flow Chart of the Numerical Algorithm

$$Sh = (0.35 + 0.56 Re^{0.52}) Sc^{0.3}. \quad (38)$$

The corresponding expression for heat transfer is obtained by the analogy between heat and mass transfer by replacing Schmidt and Sherwood numbers by Prandtl and Nusselt numbers respectively.

ii. Vapour-gas mixture viscosity,  $\mu_{vg}$ .

In this thesis, the vapour-gas mixture was considered to consist of phthalic anhydride and water vapour (i.e. neglecting any by-product like maleic anhydride). The vapour-gas mixture was treated as a binary mixture.

The viscosity of the vapour-gas mixture is calculated based on the correlation of Carr et al (1954)

$$\mu_{vg} = \frac{\sum_{i=1}^n y_i \mu_i \sqrt{M_i}}{\sum_{i=1}^n y_i \sqrt{M_i}}. \quad (39)$$

iii. Thermal conductivity of vapour-gas mixture,  $k_{vg}$ .

The thermal conductivity of a vapour-gas mixture is not generally a linear function of the composition of a vapour-gas mixture. The correlation of Lindsay and Bromley (1950) for a binary mixture has been used based on the recommendation of Reid and Sherwood (1977),

$$k_{vg} = \frac{k_i}{1 + A_{ij}(y_j/y_i)} + \frac{k_j}{1 + A_{ji}(y_i/y_j)} \quad (40)$$

where

$$A_{ij} = \frac{1}{4} \left[ 1 + \left[ \left( \frac{\mu_i}{\mu_j} \right) \left( \frac{M_j}{M_i} \right)^{0.75} \frac{1 + S_i/T}{1 + S_j/T} \right]^{0.5} \right]^2 \left[ \frac{1 + S_{ij}/T}{1 + S_i/T} \right] \quad (41)$$

$A_{ji}$  - same expression as  $A_{ij}$  with subscripts interchanged

$$S = 1.5 T_b \quad (42)$$

$$S_{ij} = 0.735 (S_i S_j)^{0.5} \quad (43)$$

where

$y_i, y_j$	=	mole fractions
$k_i, k_j$	=	thermal conductivities of pure components
$\mu_i, \mu_j$	=	viscosities of pure components
$M_i, M_j$	=	molecular weights of pure components
$T$	=	absolute temperature, K
$S_i, S_j$	=	Sutherland constants of pure components, K
$T_b$	=	normal boiling point of a pure component, K.

#### iv. Diffusion coefficient, $D_{ij}$ .

The diffusion coefficient,  $D_{ij}$ , for a binary gas mixture at pressures less than 15 atmospheres is best estimated by the Chapman-Enskog Kinetic Theory (Bird et al. (1960)) as follows:

$$D_{ij} = \frac{188.26 T^{3/2}}{P \sigma_{ij}^2 \Omega_{ij}} \sqrt{\frac{1}{M_i} + \frac{1}{M_j}} \quad (\text{cm}^2/\text{s}) \quad (44)$$

where  $\sigma_{ij}$  is collision diameter found from

$$\sigma_{i,j} = 0.833 v_{c_{i,j}}^{1/3} \quad (45)$$

and  $\Omega_{ij}$  is the collision integral (tabulated in Bird et al. (1960)) as a function of  $\frac{kT}{\epsilon_{ij}}$ . The values of  $\sigma_{ij}$  and  $\epsilon_{ij}$  may be calculated from:

$$\sigma_{ij} = 0.5 (\sigma_i + \sigma_j) \quad (46)$$

and

$$\epsilon_{ij} = \sqrt{\epsilon_i \epsilon_j} \quad (47)$$

Since most of the physical constants of phthalic anhydride are not given in the literature, they were either estimated by simple empirical relations or calculated by using atomic and structural constants which represent the component parts of the molecule.

### CHAPTER 3

#### CASE STUDIES

##### Introduction

This chapter deals with case studies which were necessary for the investigation of the effect of different factors and key parameters on the system. The results and discussions of each case studied are presented here.

The influence of volumetric flow rate, inlet temperature and type of coolant on the system are studied and analysed.

Finned tubes are specified after considering the effect of fin material, tube material and fin geometry on the rate of desublimation. Fin material and geometry affect the deposition profiles and the flow conditions of the vapour-gas mixture and the results of the model predictions are discussed in this chapter. The effects of the composition and velocity of the vapour-gas mixture on the type of desublimation applicable are presented.

The numerical estimation of the amount of solid formed is considered in the latter part of this chapter.

### Theory

Thermal diffusivity,  $\alpha = k/\rho c$ , is indicative of the rate at which a change of temperature is experienced through the medium. In effect, the thermal conductivity shows the tendency toward rapid travel of temperature change through the medium, whereas the thermal capacity varies directly as the resistance to temperature diffusion (represented by the ability of the material to absorb thermal energy during the process of a temperature change). The thermal diffusivities,  $\alpha_s$ ,  $\alpha_L$  and  $\alpha_m$  are properties of the materials, and the rate of temperature change depends on their numerical values. Qualitatively it is observed that in a material that combines a low thermal conductivity with a large specific heat per unit volume, the rate of temperature change will be slower than in a material that possesses a large thermal diffusivity.

A measure of the relative importance of the thermal resistance within the solid is the ratio of the internal to the external resistance. The external resistance is expressed in terms of the heat transfer coefficient,  $\bar{h}_c$ . The heat transfer coefficient measures the amount of heat transferred to the solid from the vapour-gas mixture at the solid-gas interface. The numerical value of  $\bar{h}_c$  in this system depends on the geometry of the surface (finned tube) and the velocity, as well as on the physical properties of the vapour-gas mixture and on the temperature difference,  $\Delta T = T_\infty - T_{des}$ . For a given value of

Nusselt number, the heat transfer coefficient,  $\bar{h}_c$ , is directly proportional to the thermal conductivity of the vapour-gas mixture.

The magnitude of the latent heat of sublimation,  $\Delta H$ , is directly related to the movement of the phase change front. If the latent heat is small, the heat released by the interface during phase change is affected very little.

The pressure,  $P$ , in the system is selected based on the P-T diagram of the desubliming component. The partial pressure is chosen such that the temperature in the solid is always less than the triple point of the desubliming component. But during the melting of the product, the partial pressure is chosen such that the temperature is equal to the melting point.

### 3.1 Physical Properties of Metal (including fins)

#### 3.1.1 Effect of Thermal Diffusivities of Metals

For this study, the tube and fins were considered to be made of the same material. To study the effect of fin material, especially thermal diffusivity on the rate of desublimation, two model predictions were made using two different low-alloy steels with thermal diffusivities of  $1.69 \times 10^{-5} \text{ m}^2/\text{s}$  and  $1.08 \times 10^{-5} \text{ m}^2/\text{s}$ . Water with an inlet temperature,  $T_c$ , of  $20^\circ\text{C}$  was used as a coolant for this study. The volumetric flow rate,  $Q$ , of the water was  $7.03 \times 10^{-5} \text{ m}^3/\text{s}$ . The fin height,  $h$ , was 20 mm and the fin pitch,  $p$ , was 23 mm. The inside

diameter of the tube was 36 mm, which was the same for all other case studies. The model predictions were being compared after a time interval of 16 minutes. This time was thought to be sufficient because the space between the fins was about 60% or more filled up with solid. As a result, this time was used as the operation time for all other cases in this model.

The time step plays a dominant role in explicit methods. Steels were selected to allow a higher time step size. This was necessary to avoid numerous computations since an explicit method was applied to this model. This indicates that denser metals were appropriate but copper, which is denser and has a higher thermal conductivity than most steel alloys, was not suitable for this study because of the small time step size.

The time step size was calculated from the stability criteria of equations (37a) and (37b) and, from observations, low-alloy steel provided a higher time step size which was necessary for explicit computation. For this study, the time step was calculated for each region (coolant, metal and solid) from the stability criteria and the smallest one was selected. It was concluded that thermal diffusivity was the most important parameter to consider when dealing with fin material with an explicit formulation. Thus thermal conductivity was an inappropriate indicator of the suitability of the fin and tube material for this study.

The heat is transferred from the vapour-gas mixture to the coolant through the metal surface and the solid layer. Here it is necessary to take account of the heat liberated during the phase transition (desublimation).

On the basis of thermal conductivity and thermal diffusivity, it is apparent from Figure 5 that the deposition profile is a strong function of the thermal properties of the fin material. This is in agreement with the Fourier number, which is a measure of the rate of heat conduction in comparison with the rate of heat storage. It is, therefore, clear that the larger the Fourier number, the deeper is the penetration of heat from the solid into the metal. This relationship also shows that the higher the Fourier number, or the thermal diffusivity, the more heat penetrates through the metal and more heat is carried away by the coolant and hence more desublimation of phthalic anhydride occurs. It is shown that when explicit methods are employed, the time step has to be strictly limited and the limitation depends on the values of the thermophysical properties. The deposition profiles are similar to those of Gorelik et al. (1980) but, since their experimental data were not supplied, it was not possible to compare the actual values. Finned tubes are constructed from most combinations of ferrous alloys, including carbon steels, stainless steels and high-grade corrosion-resistant alloys.

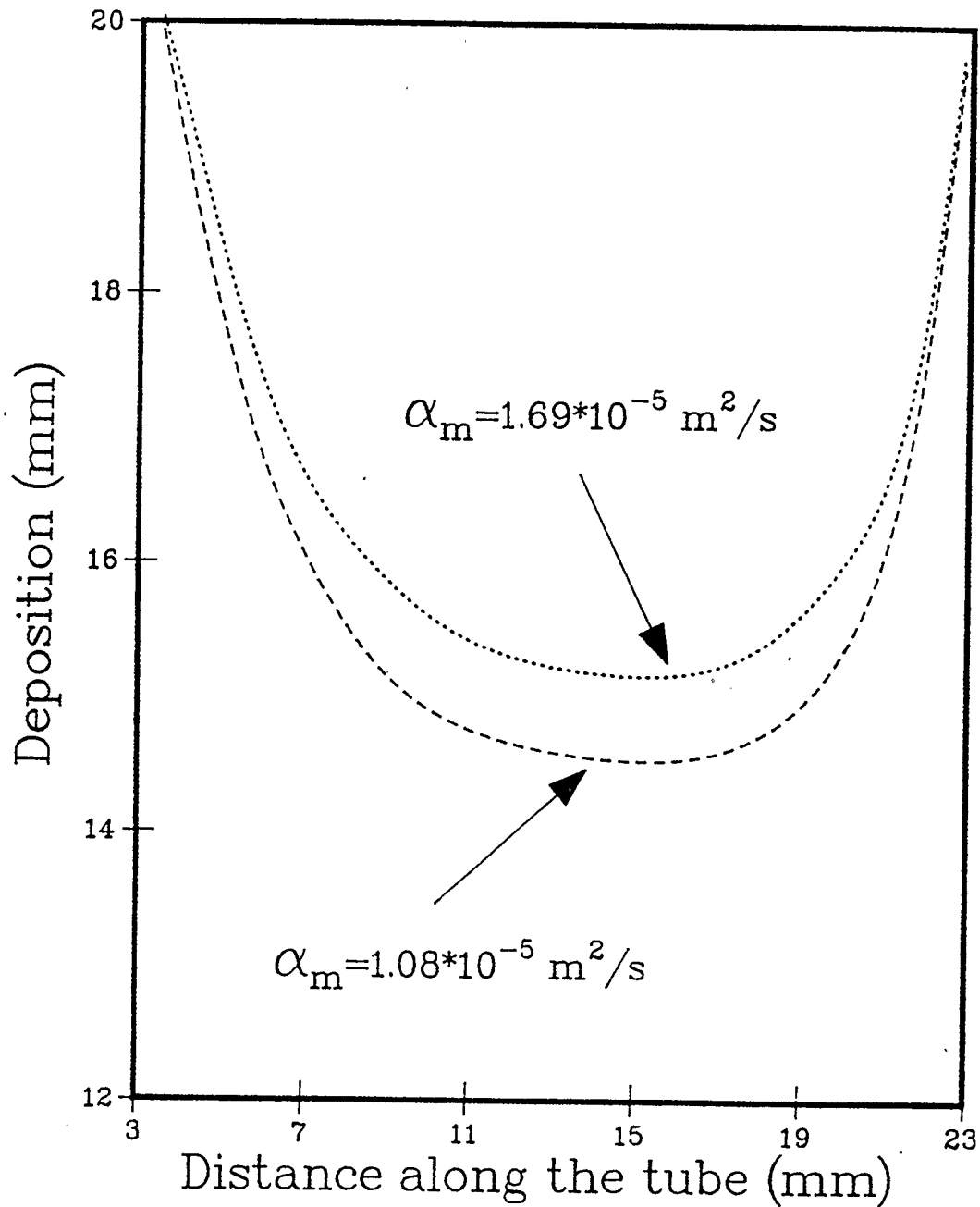


Figure 5. Effect of thermal diffusivity of the metal on deposition, water as a coolant.

### 3.1.2 Effect of Fin Height

To study the effect of fin height or the fin height-to-diameter ratio,  $h/d_o$ , on the rate of desublimation, model predictions were conducted using two different fin heights of 20 mm and 30 mm. The coolant used for each case was water with an inlet temperature of 20°C. The volumetric flow rate,  $Q$ , was  $7.03 \times 10^{-5} \text{ m}^3/\text{s}$ . The fin pitch was also the same, which was often used for most case studies in this model.

It is obvious from Figure 6 that the 30 mm fin gave a higher deposit of solid after a time interval of 16 minutes than the 20 mm fin. This shows that fin height or the fin height-to-diameter ratio ( $h/d_o$ ) plays an important role on the rate of desublimation.

For a given tube diameter there is a given range of applicable fin height. These are obtained from heat transfer correlations by Brigg and Young (1963). Some model predictions of fin heights outside the range were made, but the deposition profiles were lower than those in the given range. This implies that for a given tube diameter there is limitation to the fin height. Model predictions for fin height outside a given range indicate that it is not possible to maximize fin performance. But it is possible, however, to maximize the efficiency with respect to quality of fin material. From these model predictions it is, therefore, clear that the fin height is a key parameter in designing and constructing a desublimator for recovering sublimation

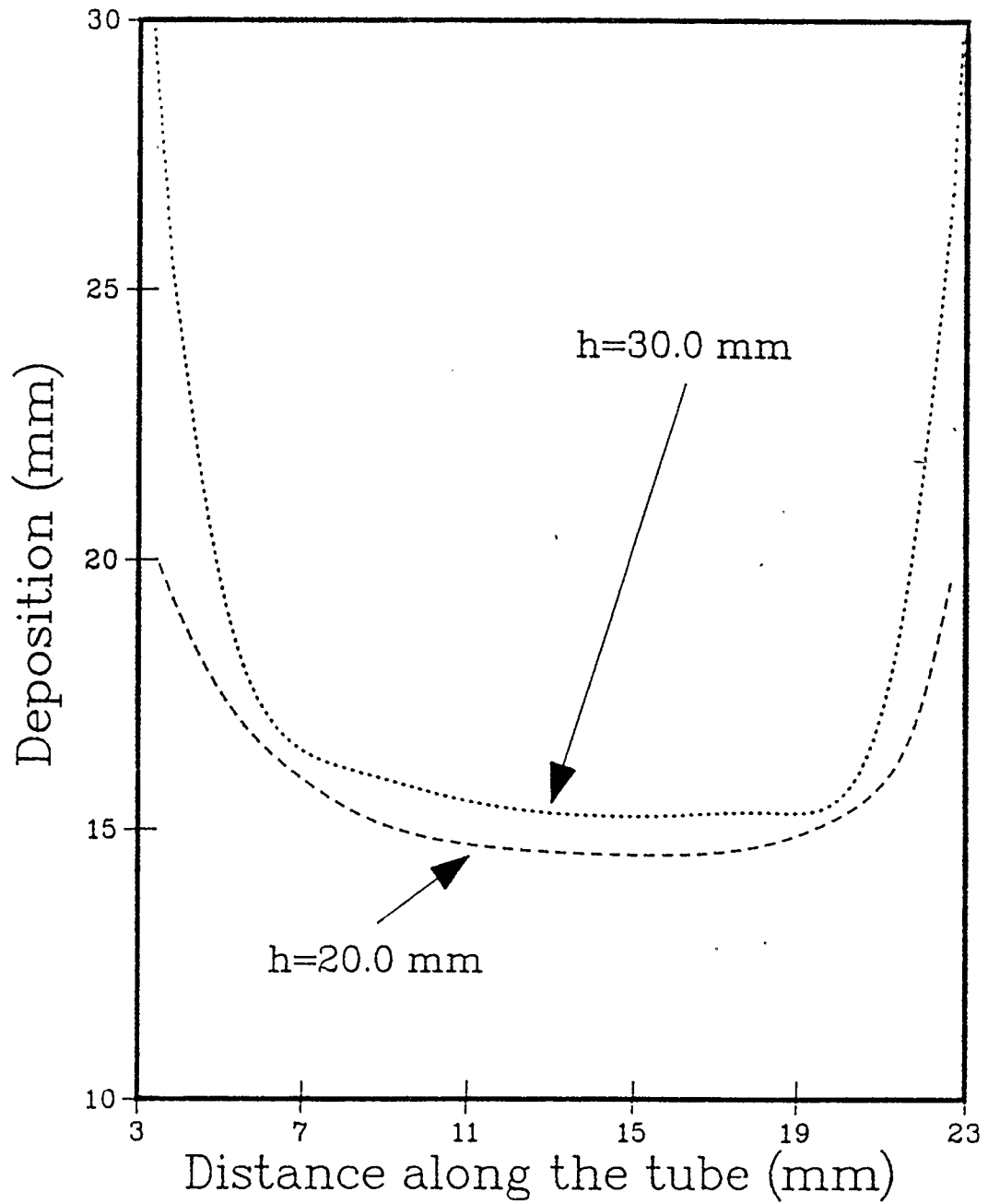


Figure 6. Effect of fin height,  $T_c=20^\circ\text{C}$ , water as a coolant,  $p=23$  mm.

products. The ratio of fin height-to-tube diameter ( $h/d_o$ ) is an important parameter to be taken into account when the conditions being designed cannot be perfectly matched to a set of conditions given by Weierman (1975) and Smittle (1980).

### 3.1.3 Effect of Fin Height-to-Pitch Ratio

In order to investigate the effect of fin height-to-pitch ratio ( $h/p$ ), model predictions were generated for two different fins with different fin pitch. This study was also necessary to study the effect of the thickness (difference between pitch and clearance) of the fins and compactness of the fins on the rate of deposition. For a fin height of 20 mm, the pitch was varied between 19 mm and 23 mm. Water was used as the coolant with an inlet temperature of  $10^{\circ}\text{C}$ . The results are given in Figure 7. This study was necessary to investigate the effect of geometry of the fin on the symmetry of the deposition profile. It is clear that for a low height-to-pitch ratio, the deposition profile is not symmetrical. This is explained by the fact that the coolant enters the tube at  $10^{\circ}\text{C}$  and warms up as it moves along the length of the tube. As a result, the higher the fin pitch, the more the coolant becomes heated and, therefore, less deposition occurs. This indicates that there is high deposition just after the entrance of the tube, but for high  $h/p$  the deposition profile appears to become more symmetrical. For a given diameter there is a given range of  $h/p$  applicable. Fin pitch and height can be varied to achieve the proper outside-to-inside surface ratio.

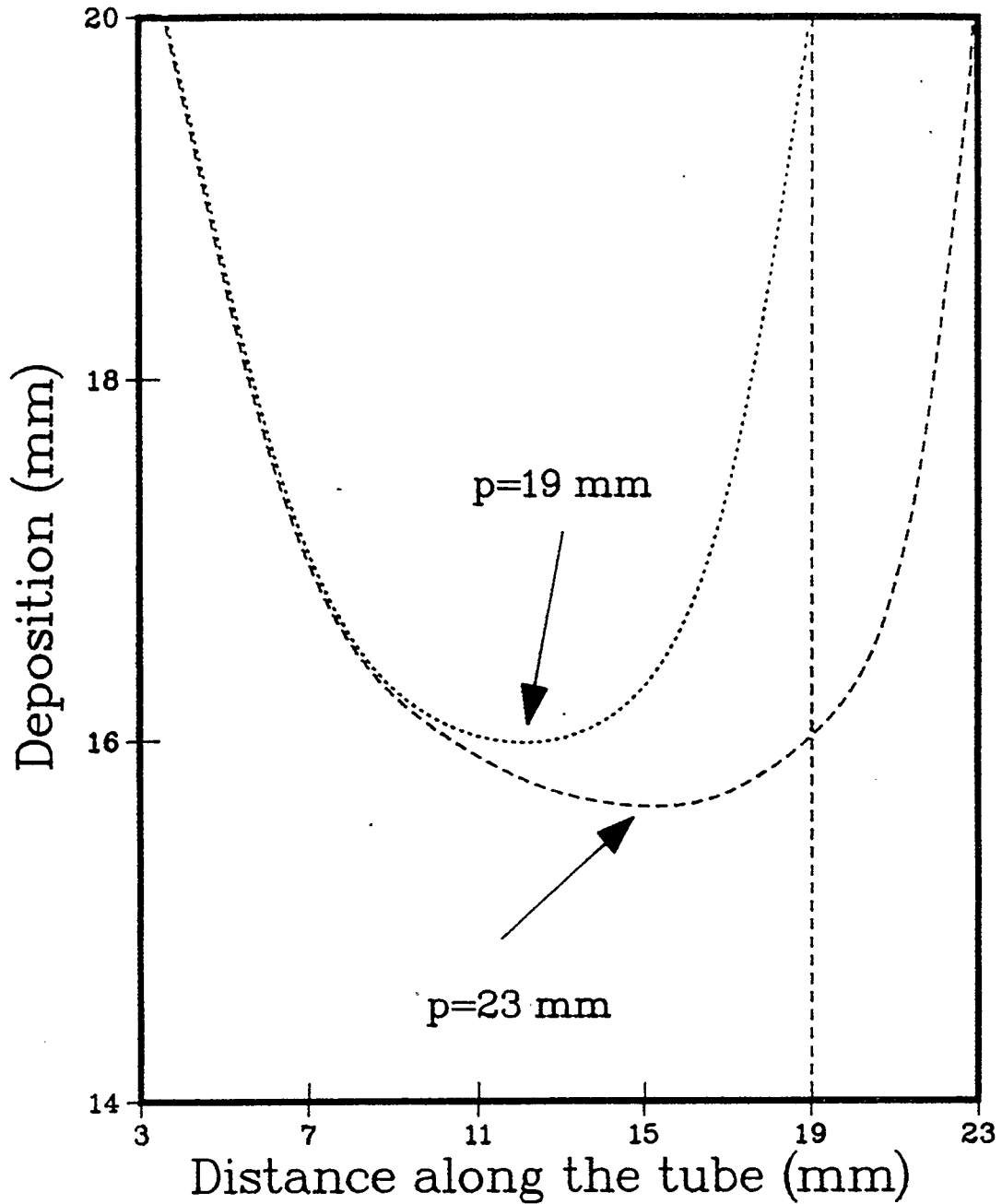


Figure 7. Effect of height-to-pitch ratio on the deposition profile,  $T_c=10^\circ\text{C}$ ,  $t=16$  min.,  $h=20$  mm.

### 3.2 Effect of Time on Development of the Deposition Profile

To investigate the effect of time on the development of the deposition profile, model predictions were studied for different time intervals (4, 8, and 16 minutes). Figure 8 shows deposition profiles for different time intervals when water with an inlet temperature of  $10^{\circ}\text{C}$  was used. Other operating conditions were  $h = 20 \text{ mm}$ ,  $p = 19 \text{ mm}$  and  $Q = 7 \times 10^{-5} \text{ m}^3/\text{s}$ . This figure gives an idea about the development of the deposition profile with time. The deposition profile is in the form a curve because of the two-dimensional temperature gradient in the system. It is clear that the deposition profile is fully developed at  $t = 16$  minutes. The same trend is noticed in Figure 9 which represents the results of model predictions conducted under the following operating conditions:

$$p = 23 \text{ mm}$$

$$T_c = 20^{\circ}\text{C} .$$

The rest of the operating conditions were the same. The deposition profiles for  $t = 4$  and 8 minutes in Figure 8 are more symmetrical than those in Figure 9. This is due to the difference in fin pitch which is explained under Section 3.1.3. It is therefore clear from these two figures that the nature and development of the deposition profile is a function of time and distance along the tube.

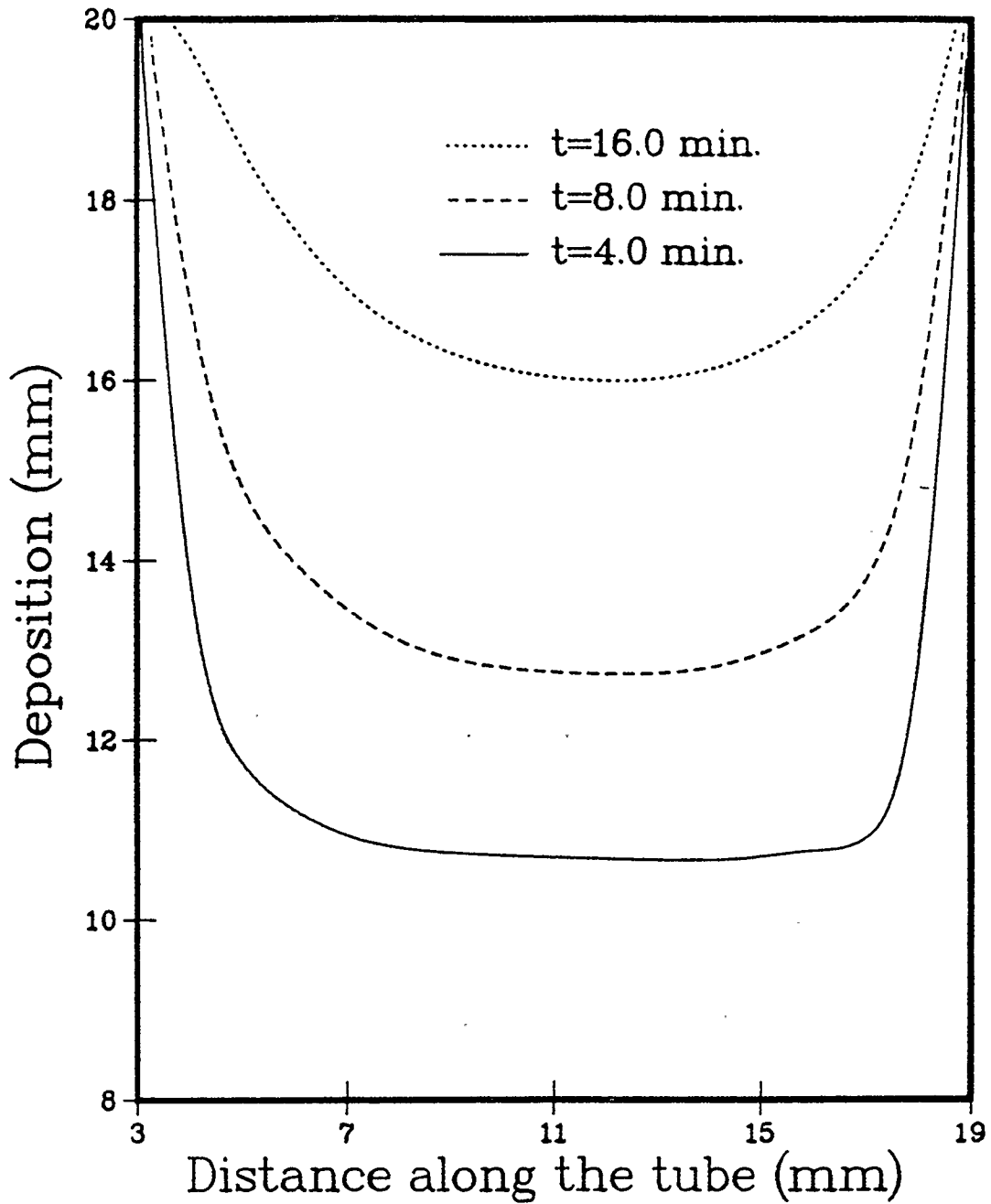


Figure 8. Deposition as a function of time, water as a coolant,  $h=20$  mm.,  $p=19$  mm.,  $T_c=10^\circ\text{C}$ .

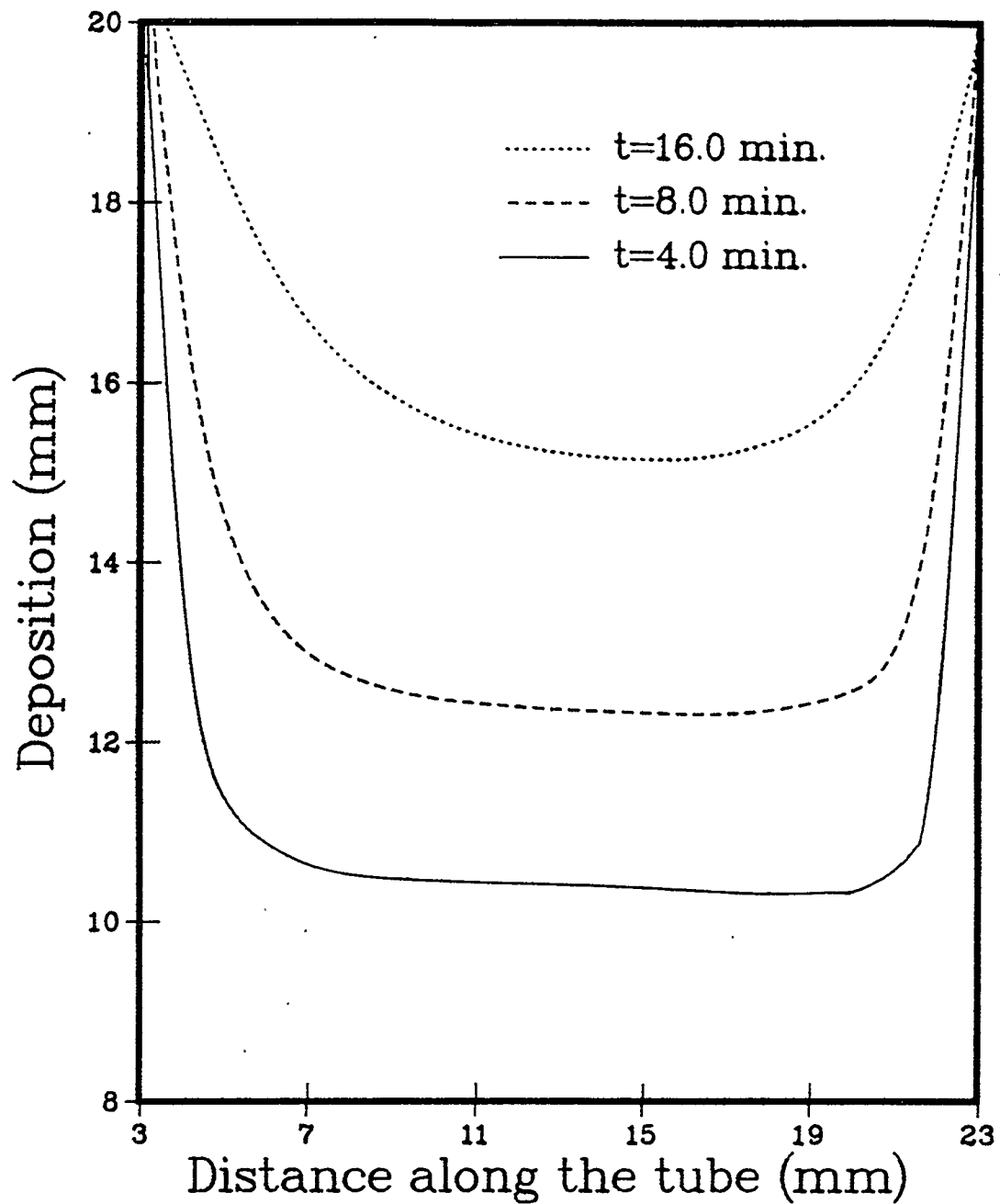


Figure 9. Deposition as a function of time, water as a coolant,  $h=20$  mm.,  $p=23$  mm.,  $T_c=20^\circ\text{C}$ .

### 3.3 Effect of Coolant Properties

#### 3.3.1 Effect of Inlet Temperature of Coolant

Model predictions were obtained for different coolants with different inlet temperatures in order to elucidate the influence of inlet temperature on the rate of desublimation. Figure 10 shows the effect of inlet temperature on the rate of deposition when ethylene glycol was used as a coolant. For this case, three different inlet temperatures were chosen ( $10^{\circ}\text{C}$ ,  $20^{\circ}\text{C}$  and  $40^{\circ}\text{C}$ ). It is clear that the lower the inlet temperature, the greater the temperature gradient between the desublimation temperature,  $T_{\text{des}}$ , and the inlet temperature of ethylene glycol. Therefore, at lower inlet temperatures, more heat is conducted through the solid, metal and finally through the coolant. Similar results were obtained for water and o-xylene at the same set of inlet temperatures. The results are shown in Figures 11 and 12. The same dependency was noticed. It is, therefore, clear that the inlet temperature plays a very important role in desublimation.

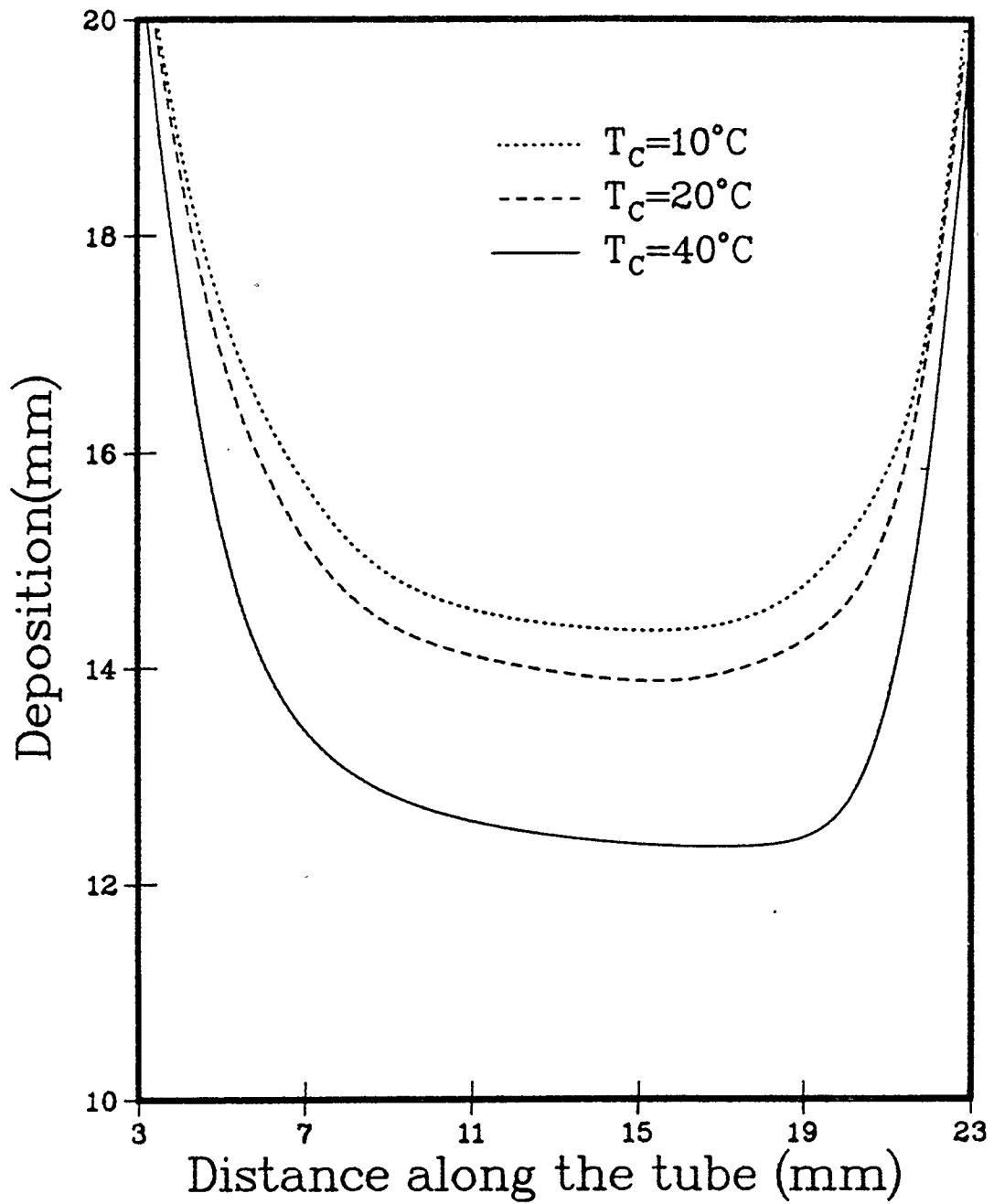


Figure 10. Effect of inlet temperature of ethylene glycol,  $h=20$  mm.,  $p=23$  mm.,  $t=16$  min.

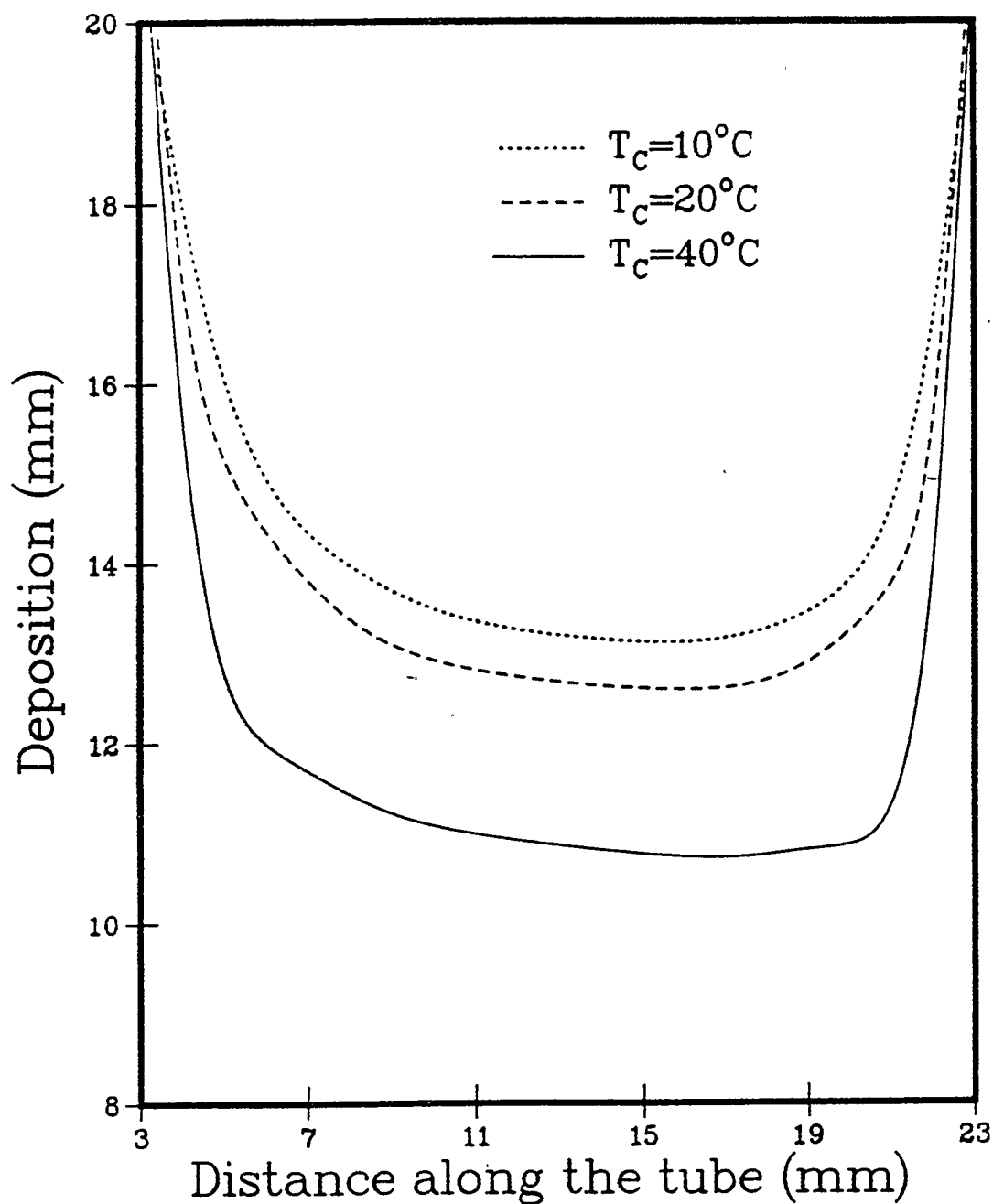


Figure 11. Effect of inlet temperature of o-xylene on deposition,  $t=16$  min.  $h=20$  mm.

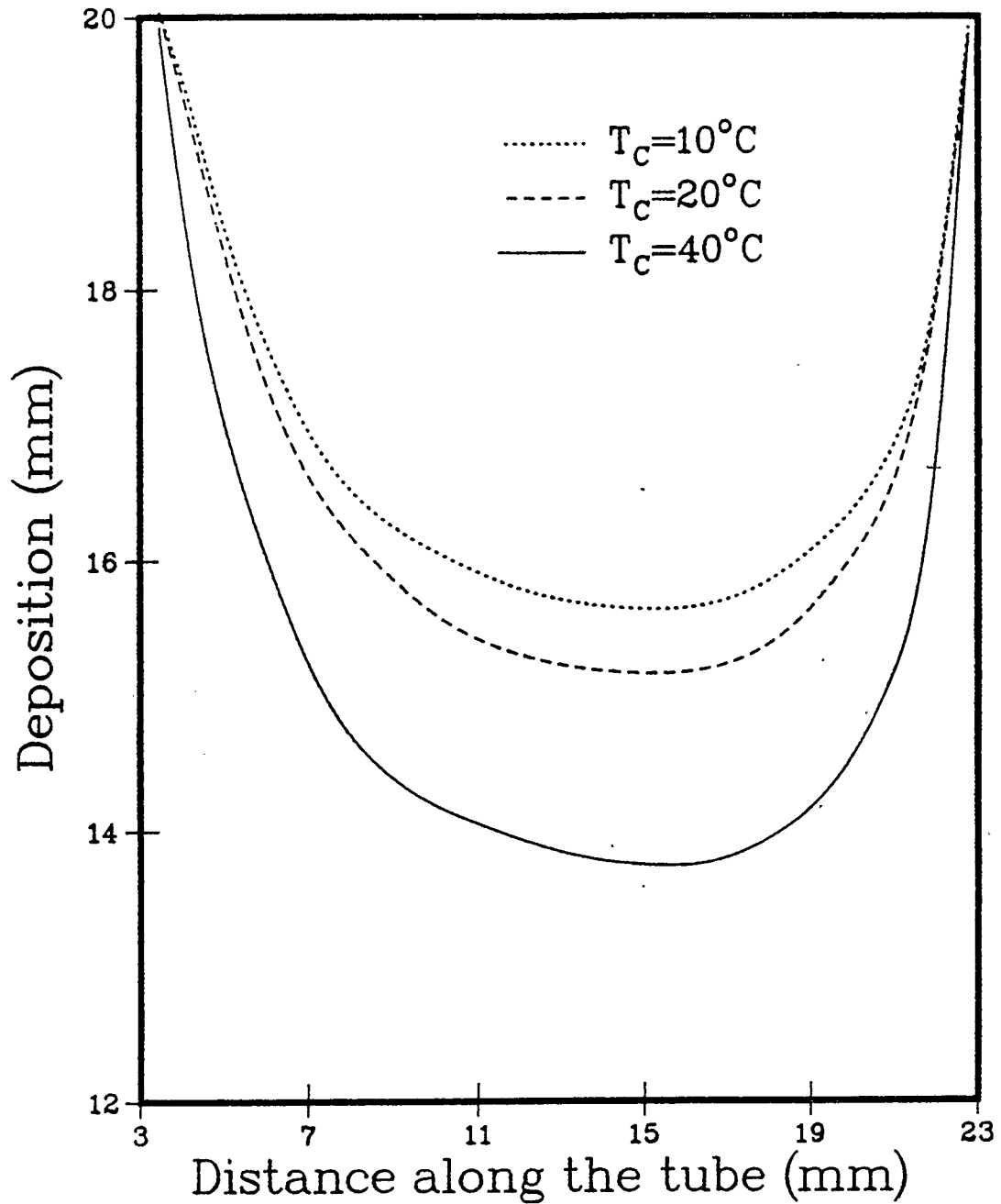


Figure 12. Effect of inlet temperature of water on deposition,  $t=16$  min.,  $p=23$  mm.,  $h=20$  mm.

### 3.3.2 Effect of Type of Coolant

In order to study the effect of the type of coolant on the rate of desublimation, model predictions for water, ethylene glycol and o-xylene were conducted for three different inlet temperatures. Figure 13 shows the effect of coolant on deposition at time = 16 minutes. The inlet temperature for each coolant was 10°C. It is clear that the type of coolant plays an important role on deposition. Water gives the highest deposition followed by ethylene glycol and o-xylene. This tendency is explained by the physical properties of the coolants at a particular inlet temperature. The thermal diffusivities of the above mentioned coolants follow this order

$$\alpha_{\text{water}} > \alpha_{\text{ethylene glycol}} > \alpha_{\text{o-xylene}} \quad (48)$$

From Figure 13 it is clear that the thickness of solid deposited at the location  $z = 10$  mm is 16 mm using water as a coolant and 13 mm with o-xylene. This corresponds to a 23% increase in deposition with water over o-xylene. This percentage change in deposition corresponds to a 7% increase in the thermal diffusivity of water over o-xylene.

Figure 14 shows the comparison of deposition profiles for the same coolants with the same trend. The coolant inlet temperatures was 20°C. Figure 15 shows the deposition profiles for an inlet temperature of 40°C. The same trend of deposition profile is noticed in each case.

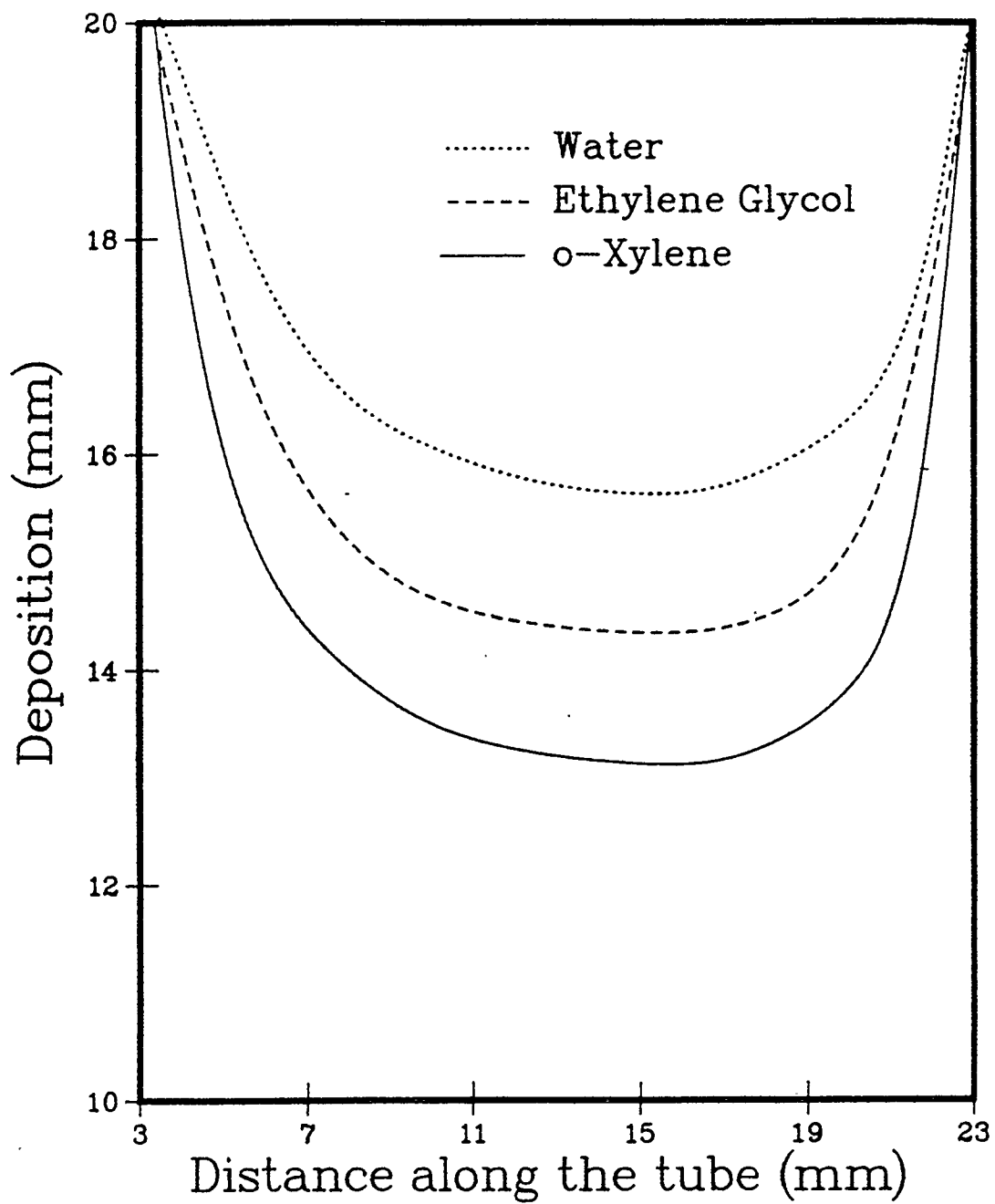


Figure 13. Effect of coolant,  $p=23$  mm.,  $h=20$  mm.,  $t=16$  min.,  $T_c=10^\circ\text{C}$ .

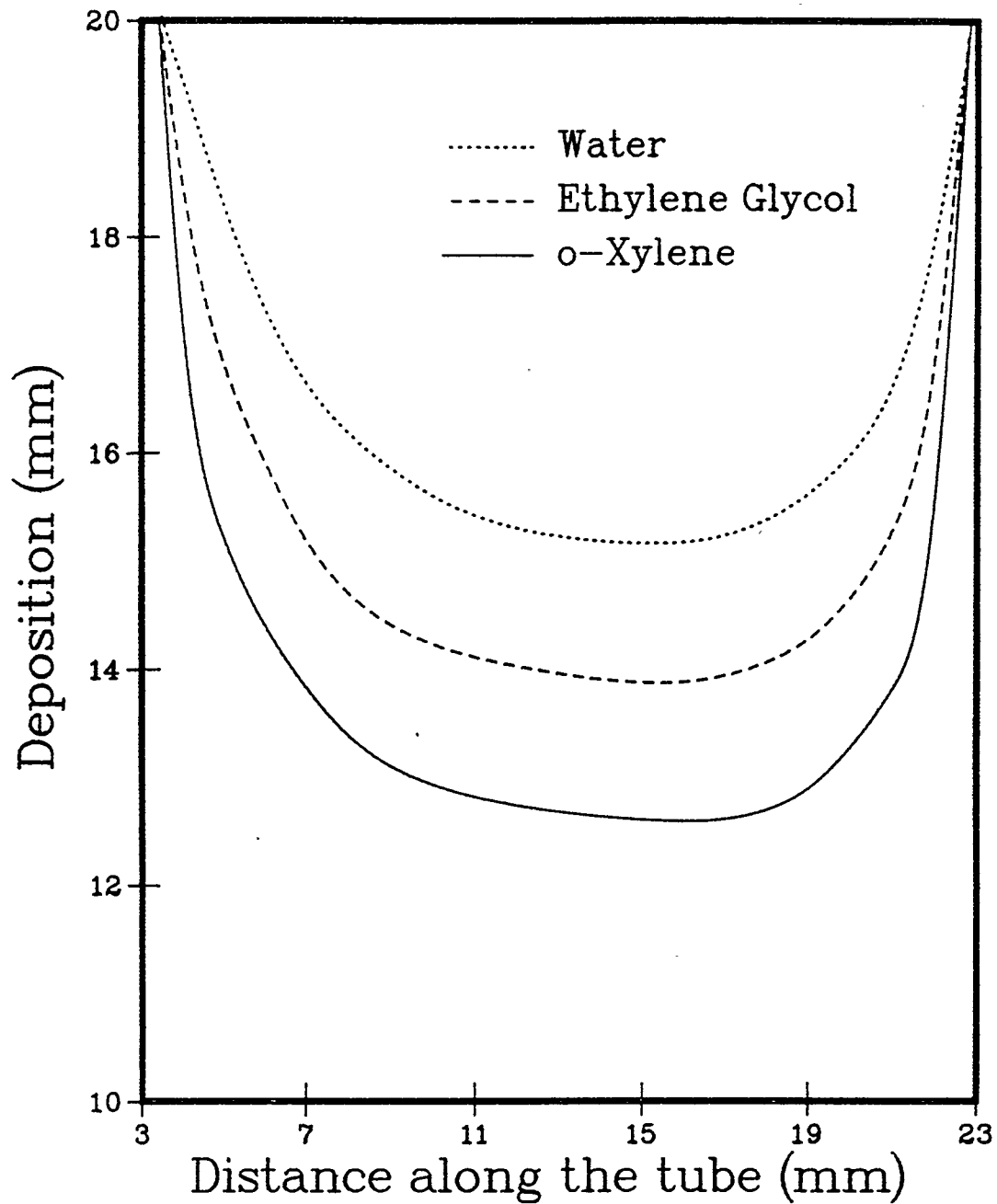


Figure 14. Effect of coolant on deposition,  $p=23$  mm.,  $h=20$  mm.,  $T_c=20^\circ\text{C}$ ,  $t=16$  min.

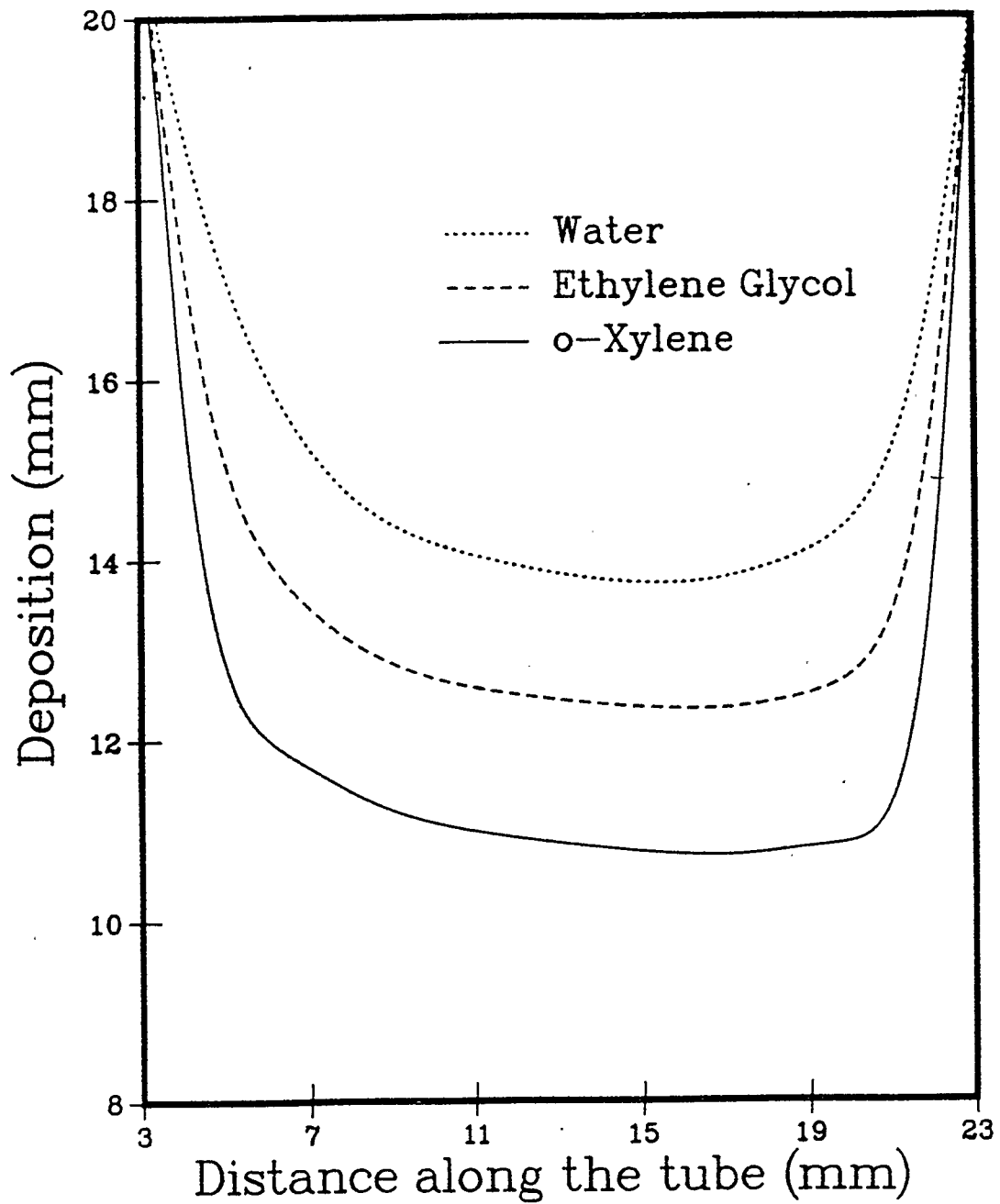


Figure 15. Effect of coolant on deposition profile,  $h=20$  mm.,  $T_c=40^\circ\text{C}$ ,  $p=23$  mm.,  $t=16$  min.

As a result of this study, coolant can be selected according to inlet temperature. The inlet temperature of the coolant is also chosen based on the desublimation temperature of the target product (phthalic anhydride for this study). For sublimation products which have desublimation temperatures higher than 60°C, it is not advisable to use water. For such cases oil, rather than water, is recommended since the thermal shocks are smaller and corrosion problems are avoided. The use of oil eliminates scaling and fouling of the tubes due to deposits.

### 3.3.3 Effect of Flow Rate

To investigate the effect of volumetric flow rate of the coolant on deposition, model predictions were generated using water as a coolant. The inlet temperature of the water was 20°C. Two values of volumetric flow rates were used for this study ( $7.03 \times 10^{-5}$  and  $3.02 \times 10^{-5} \text{ m}^3/\text{s}$ ). These values were selected to meet the recommendation of Gorelik et al. (1980). Model predictions were carried out by keeping the inner diameter of the tube constant and changing the volumetric flow rate. It was also possible to keep the volumetric flow rate constant and vary the inner diameter of the tube. Because of the computation time, the inner diameter of the tube was kept constant to use a low number of grid points in the coolant and in the system as a whole. From Figure 16, it is clear that the higher the volumetric flow rate of coolant, the more heat is removed from the solid and metal. This increases the temperature gradient and hence, more phthalic anhydride desublimates.

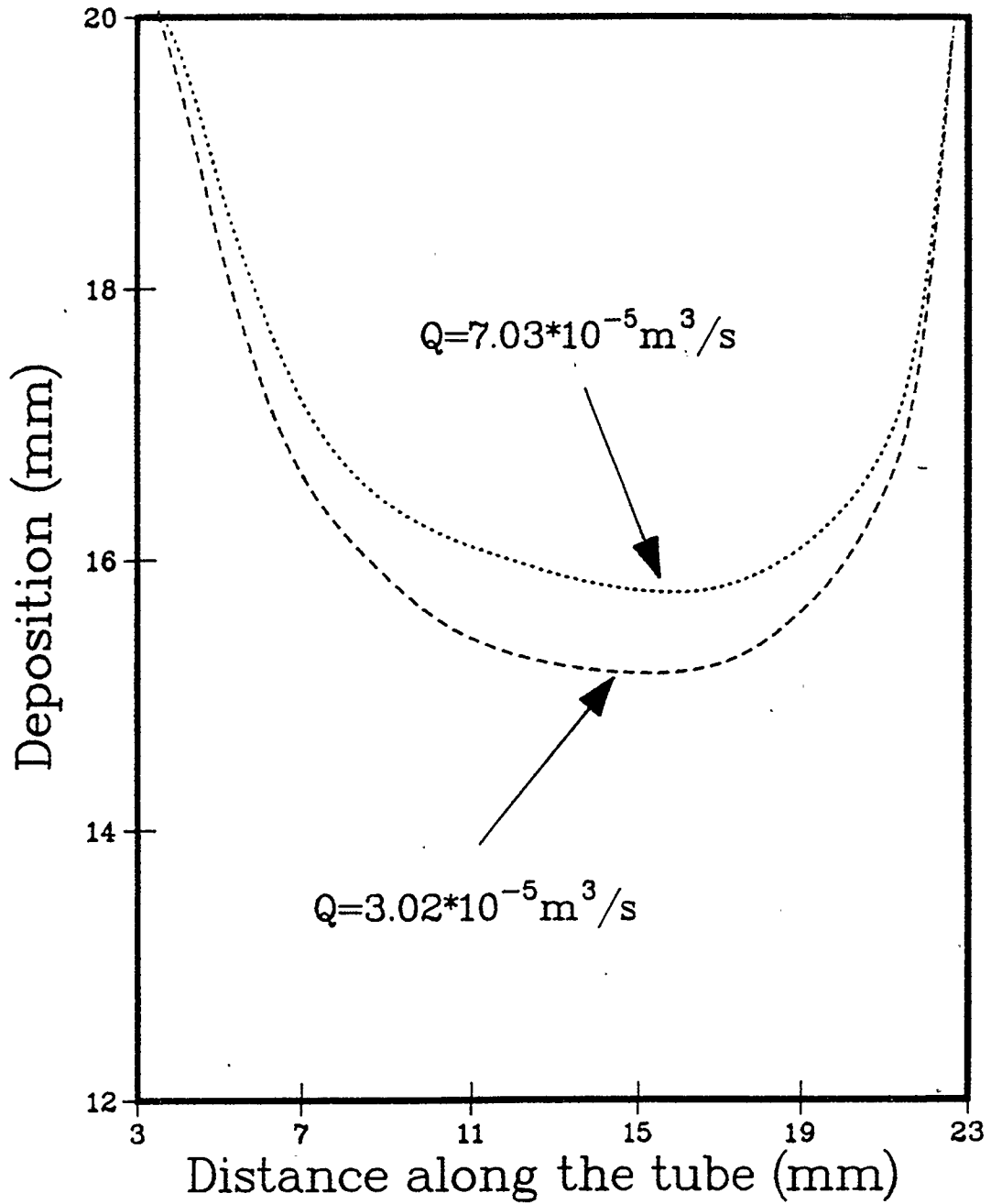


Figure 16. Comparison of deposition of different flow rates,  $h=20$  mm.,  $p=23$  mm.,  $t=16$  min.,  $T_c=20^\circ\text{C}$ .

For a given inner tube diameter, there is a given range of flow velocities. Model predictions of values outside the given range are meaningless. The range corresponds to truly laminar flow during heat transfer which, in practice, is difficult except in very small tubes. This avoids turbulence which necessitates the use of equation (5). Otherwise, equation (5a) is used.

### 3.4 Properties of Phthalic Anhydride

#### 3.4.1 Effect of Thermal Properties of Phthalic Anhydride

In order to elucidate the effect of the thermal properties of the target product on the deposition profile, model predictions at time = 16 minutes were obtained with different thermal diffusivities ( $\alpha_s = 1.7 \times 10^{-8}$ ,  $0.8 \alpha_s = 1.4 \times 10^{-8}$ , and  $5\alpha_s = 8.5 \times 10^{-8} \text{ m}^2/\text{s}$ ). The other operating conditions were,  $p = 23 \text{ mm}$ ,  $h = 20 \text{ mm}$ , and inlet temperature was  $20^\circ\text{C}$ . Water was used as a coolant.

It is clear from Figure 17 that the higher the thermal diffusivity, the higher the deposition under the above mentioned conditions. It is necessary to know the operation time and the correct fin dimensions to select. From this study, it is possible to obtain the time to start melting the target product formed on the finned tubes. It is apparent, therefore, that for a given fin size, a different amount of desublimed target product is formed, depending upon

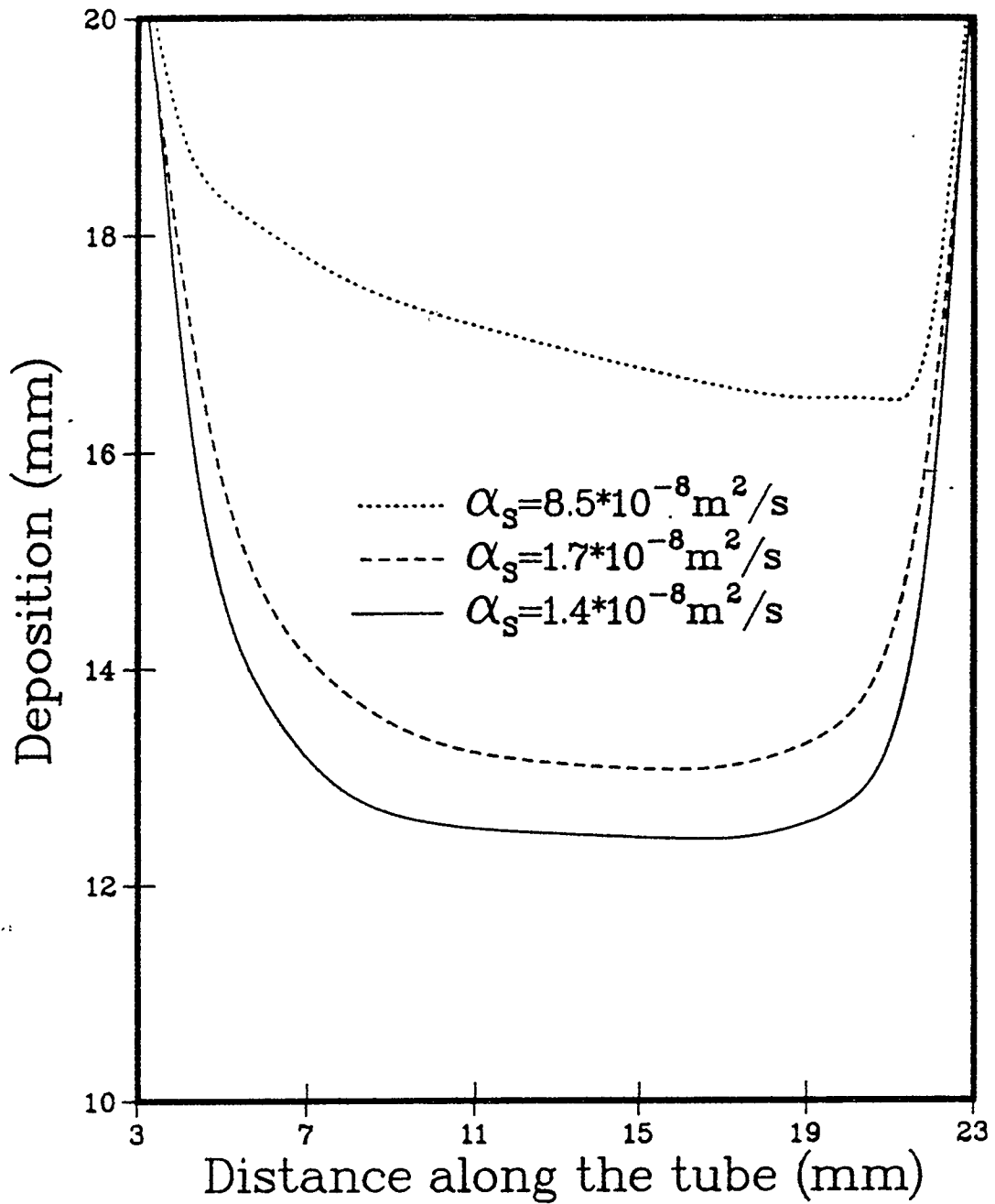


Figure 17. Effect of physical properties of solid on deposition,  $p=23$  mm.,  $h=20$  mm.,  $t=16$  min.,  $T_c=20^\circ\text{C}$ .

its physical properties. This study is especially useful if a different sublimation product is to be desublimed on the same finned tube banks.

### 3.5 Properties of Vapour-Gas Mixture

#### 3.5.1 Effect of Composition and Velocity of Vapour-Gas Mixture

To elucidate the influence of composition and velocity of the vapour-gas mixture, model predictions with different velocities and compositions were compared. Figure 18 shows predictions for three different mole fractions (0.08, 0.09 and 0.1) of phthalic anhydride in the vapour-gas mixture. The vapour-gas velocity was taken as 15 m/s as an example. The results show that for higher mole fractions the rate of desublimation is higher.

To study the influence of vapour-gas velocity on the rate of desublimation, model predictions of different vapour-gas velocities were conducted. The results are shown in Figure 19. This figure shows the relationship between vapour-gas velocities and the rate of desublimation. The values on the ordinate represent the difference between the rate of mass flux,  $Y'$ , at the solid-gas interface and the rate of deposition,  $dY/dt$ . The rate of mass flux was calculated using the equation below.

$$Y' = \frac{M}{\rho_s} F \ln \frac{1 - X_{AS}}{1 - X_{AO}} \quad (49)$$

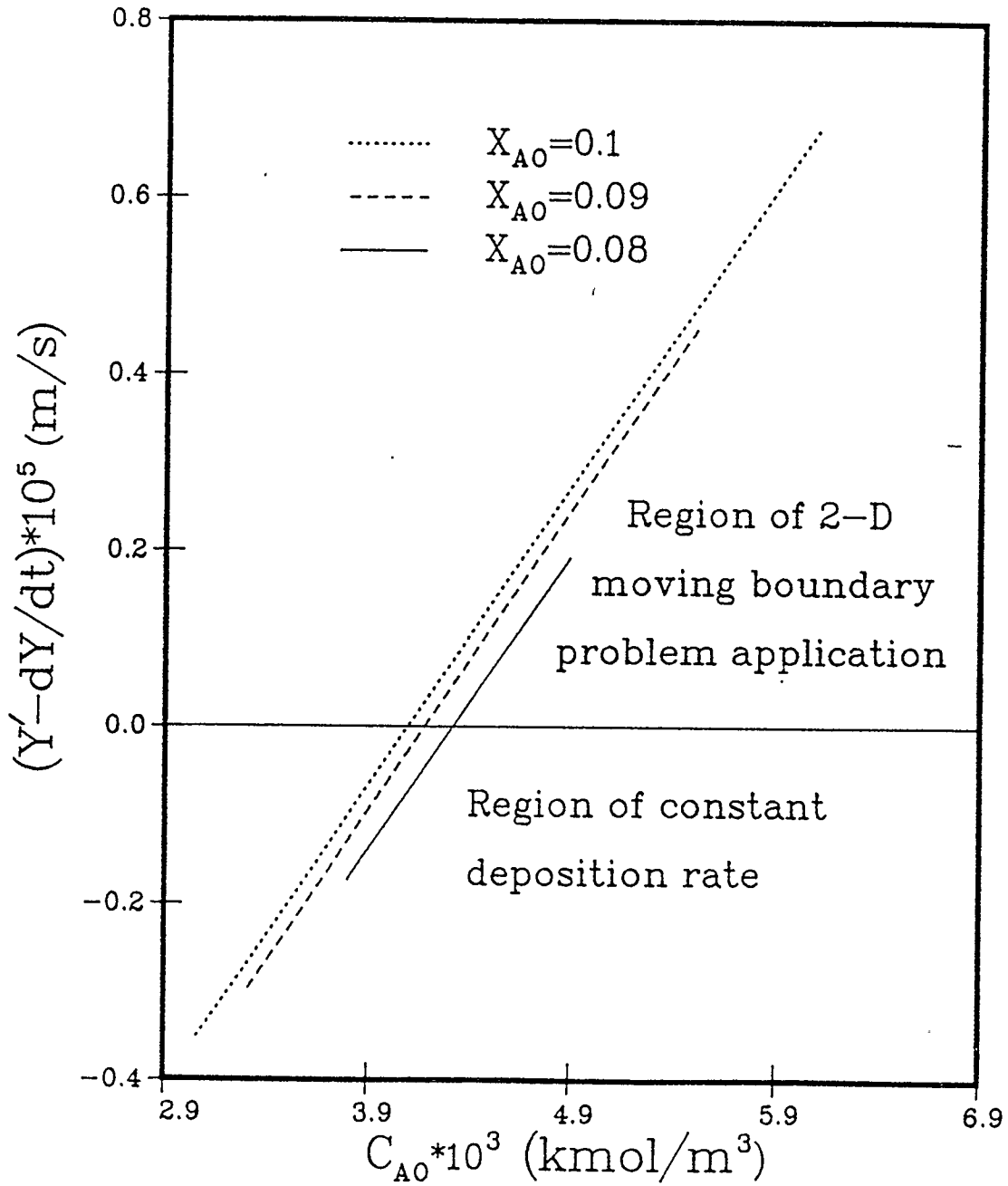


Figure 18. Effect of composition of vapour-gas mixture on deposition,  $V_{vg} = 15$  m/s.

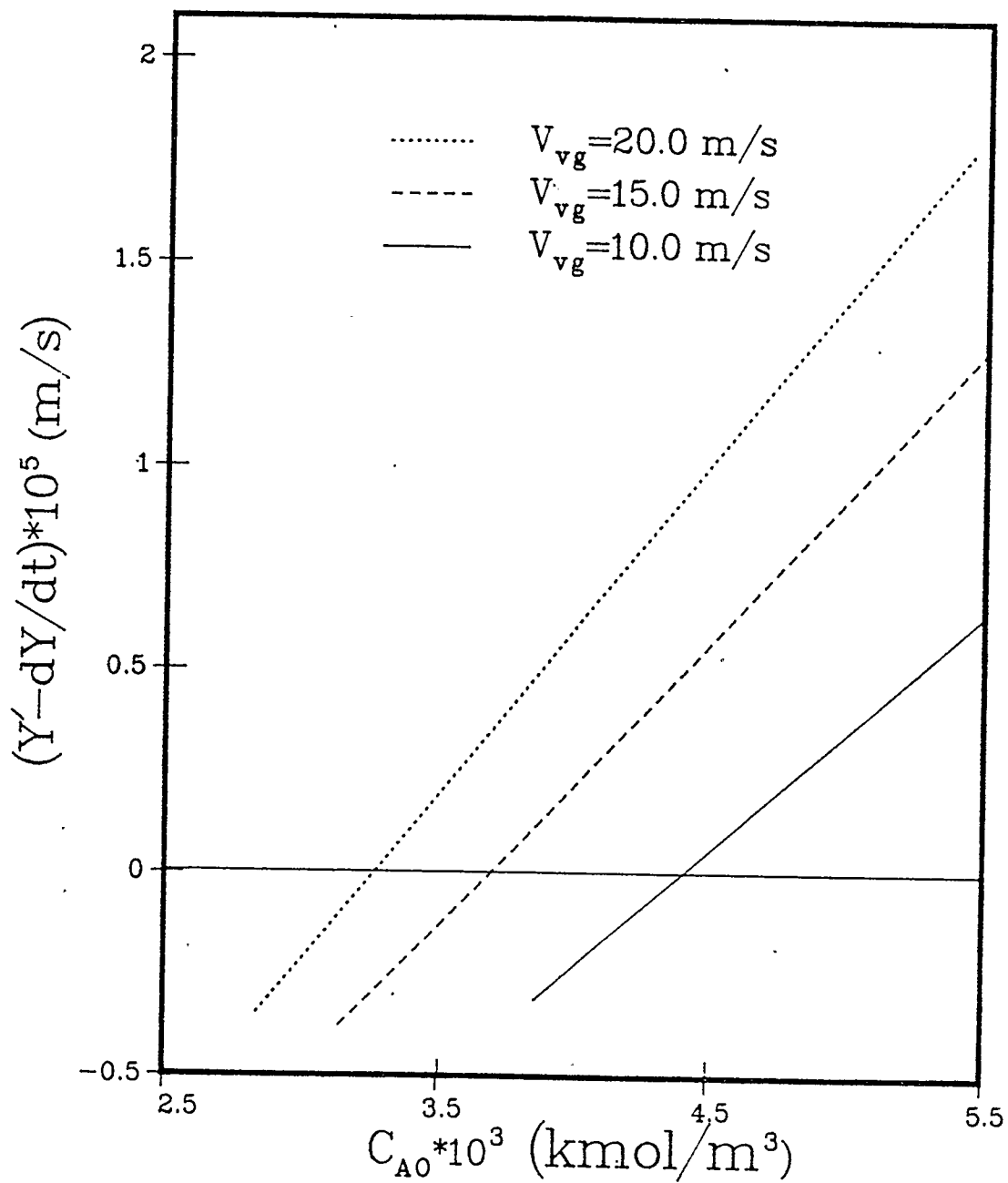


Figure 19. Effect of vapour-gas velocity on deposition,  $X_{A0} = 0.09$ .

The rate of deposition,  $dY/dt$ , was obtained by taking the maximum thickness obtained for any of the points along the tube and dividing by the time interval to obtain that thickness. There is a recommended range of vapour-gas velocities (5-20 m/s) in the literature by Gorelik et al. (1980). Figures 18 and 19 give information about the type of desublimation applicable for a given mole fraction of phthalic anhydride and the velocity of the vapour-gas mixture. Negative values of the ordinate indicate that the application of a constant deposition rate would suffice (i.e. one-dimensional desublimation). On the other hand, positive values indicate that it is necessary to study a two-dimensional moving boundary desublimation problem. Only the region of positive ordinate values was considered in this study. The results show that for high velocities it is easy to enter into the two-dimensional moving boundary desublimation region at low concentrations of phthalic anhydride in the vapour-gas mixture. This also shows that for a given mole fraction of phthalic anhydride in the vapour-gas mixture, the tendency to enter into the 2-D region is given as follows:

$$V_{vg} = 20 > V_{vg} = 15 > V_{vg} = 10 \text{ m/s} . \quad (50)$$

This study was carried out at a constant mole fraction of phthalic anhydride ( $X_{A0} = 0.09$ ). It is obvious, therefore, that the flow conditions affect the heat transfer across finned tubes and the parameters for the flow conditions are the physical properties and the

velocity of the vapour-gas mixture across the tube bank. The results of this case confirm the results reported by Gevorkyan et al (1980).

### 3.6 Temperature Profiles in the Coolant

The temperatures in the coolant were obtained for water with  $h = 20$  mm,  $p = 23$  mm,  $t = 16$  minutes, and  $T_c = 10^\circ\text{C}$ ,  $Q = 7.03 \times 10^{-5} \text{ m}^3/\text{s}$ .

Grid points were selected at three different radial distances of 0, 8 and 16 mm from the centre of the tube. The temperatures at these points were then studied in the axial direction. The results are shown in Figure 20. It is obvious that the temperatures at  $r = 8$  mm are close to those at  $r = 0$ . The temperatures at  $r = 16$  mm rise very sharply. This is explained by the big difference between the desublimation and inlet temperatures.

Figure 21 shows the results of a study with the same operating conditions as those discussed previously but with an inlet water temperature of  $40^\circ\text{C}$ . From this it is clear that the temperature profiles are close to each other. This is explained by the fact that the desublimation temperature is close to the inlet temperature.

### 3.7 Study of Isothermal Lines

To study the temperature distribution in the system, model predictions were obtained to plot isothermal lines for  $28^\circ\text{C}$ ,  $38^\circ\text{C}$ ,  $48^\circ\text{C}$ ,  $58^\circ\text{C}$  and  $60^\circ\text{C}$ . Water was used as a coolant. The other operating

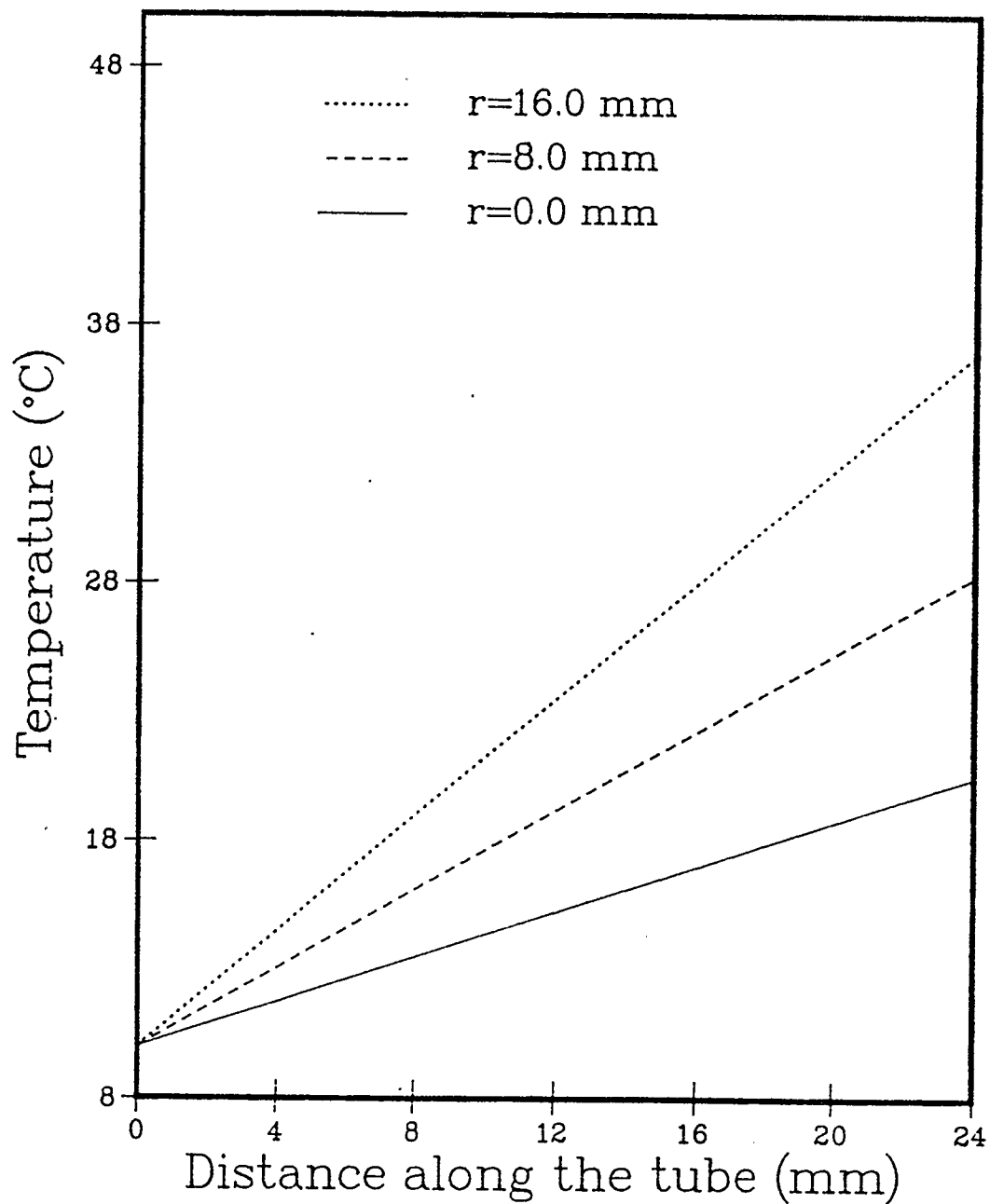


Figure 20. Temperature profile of coolant(water),  $h=20$  mm.,  $p=23$  mm.,  $t=16$  min.,  $T_c=10^\circ\text{C}$ ,  $Q=7.03 \times 10^{-5} \text{m}^3/\text{s}$ .

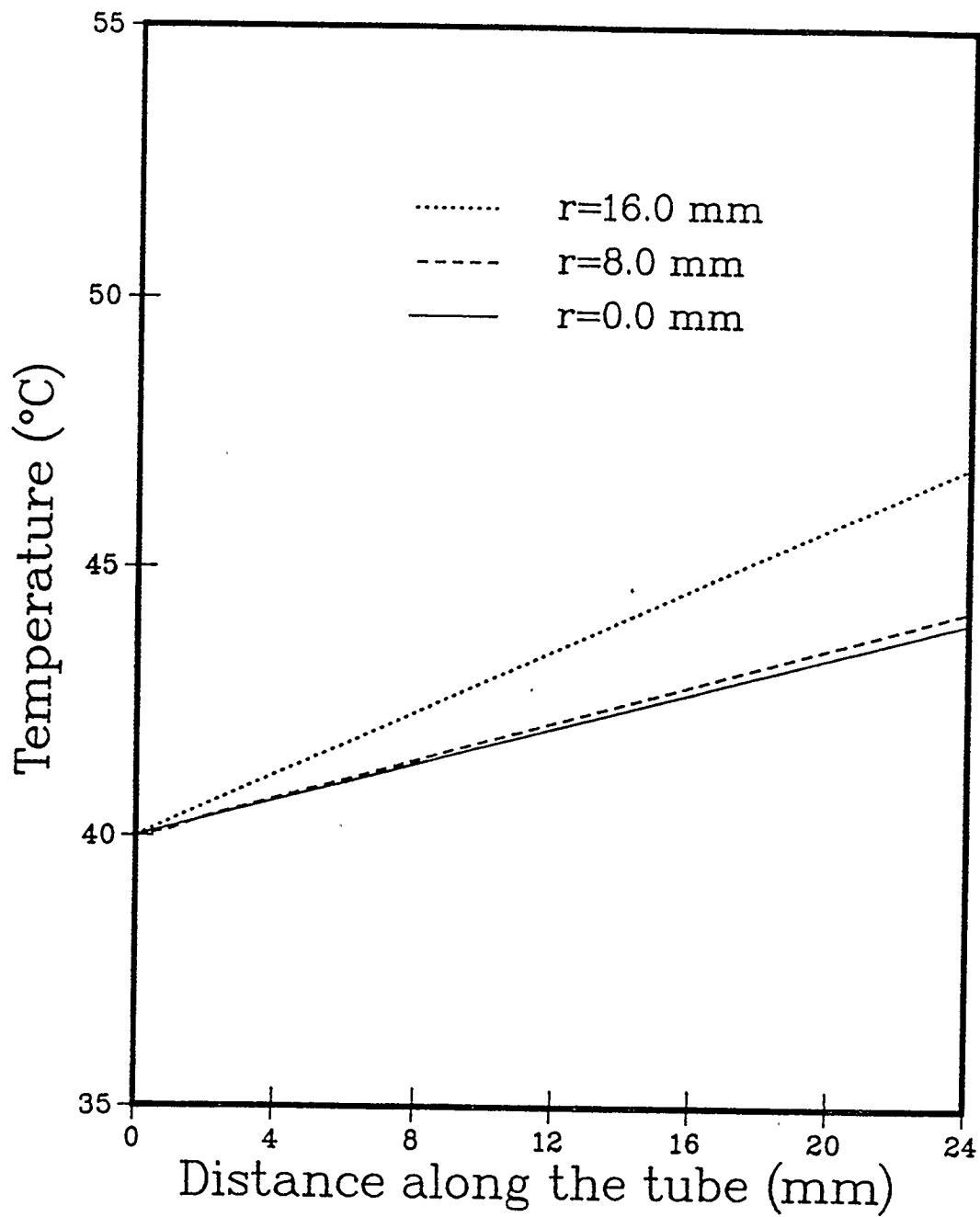


Figure 21. Temperature profile of coolant(water),  $h=20$  mm.,  $p=23$  mm.,  $t=16$  min.,  $T_c=40^\circ\text{C}$ ,  $Q=7.03 \cdot 10^{-5} \text{m}^3/\text{s}$ .

conditions were  $Q = 7.03 \times 10^{-5} \text{ m}^3/\text{s}$ ,  $T_c = 20^\circ\text{C}$ ,  $p = 23 \text{ mm}$  and  $h = 20 \text{ mm}$ .

This study was carried out by finding the locations of the above mentioned temperatures in the radial direction by interpolation and plotting these values versus distance along the centre of the tube in the direction of flow of coolant. Figure 22 shows isothermal lines. The  $60^\circ\text{C}$  isothermal line is the location of the solid-gas interface. The  $58^\circ\text{C}$  isothermal line is located in the solid and fins. The  $48^\circ\text{C}$  isothermal line starts from the metal and continues through the water. The  $28^\circ\text{C}$  and  $38^\circ\text{C}$  isotherms are confined only in the water. In order to study the effect of volumetric flow rate on isothermal lines, model predictions were conducted with a lower volumetric flow rate of  $3.02 \times 10^{-5} \text{ m}^3/\text{s}$  with other operating conditions being the same. Isothermal lines obtained are shown in Figure 23. The  $60^\circ\text{C}$ ,  $58^\circ\text{C}$ ,  $48^\circ\text{C}$  and  $38^\circ\text{C}$  isothermal lines follow the same trend as those shown in Figure 22. The  $28^\circ\text{C}$  isothermal line ends at about  $r = 1.8 \text{ mm}$  and  $z = 12 \text{ mm}$ . By comparing the  $28^\circ\text{C}$ ,  $38^\circ\text{C}$  and  $48^\circ\text{C}$  isothermal lines in Figure 22 with those in Figure 23, it is obvious that the former are located further away from the centre of the tube compared to the latter. This is explained by the low volumetric flow rate.

To elucidate the effect of fin pitch on isothermal lines, model predictions were obtained with the following conditions:  $Q = 7.03 \times 10^{-5} \text{ m}^3/\text{s}$ ,  $p = 19 \text{ mm}$ ,  $h = 20 \text{ mm}$  and  $T_c = 10^\circ\text{C}$ .

The results are shown in Figure 24. The profiles of the isothermal lines follow the same trend as those shown in Figures 22, and 23. The 48°C isothermal line starts from the fin, and continues through the solid, metal and water. The 48°C isothermal line in Figure 24 shows sharp changes in slope at the fin-solid and the coolant-metal interfaces. The slope at the coolant-metal interface is steeper because of the high temperature gradient between the metal and the water.

To study the influence of the inlet temperature of the water on the isothermal lines, an inlet temperature of 20°C was selected as another case. The operating conditions were:  $p = 19 \text{ mm}$ ,  $h = 20 \text{ mm}$ , and  $Q = 7.03 \times 10^{-5} \text{ m}^3/\text{s}$ . The results are shown in Figure 25. It is clear from Figures 24 and 25 that the 28°C, 38°C and 48°C isothermal lines of Figure 24 are located further away from the centre of the tube than those of Figure 25. This is due to the inlet temperature of water.

The inlet temperature of the water was reduced to 10°C and model predictions were generated. The results are shown in Figure 26. By comparing the isothermal lines of Figure 22 with those of Figure 26, it is clear that the 28°C, 38°C, 48°C and 58°C isothermal lines of the latter are located further away from the centre of the tube than those of Figure 22. The 48°C isothermal line of Figure 26 starts from the metal, changes slope at the metal-water interface and continues through

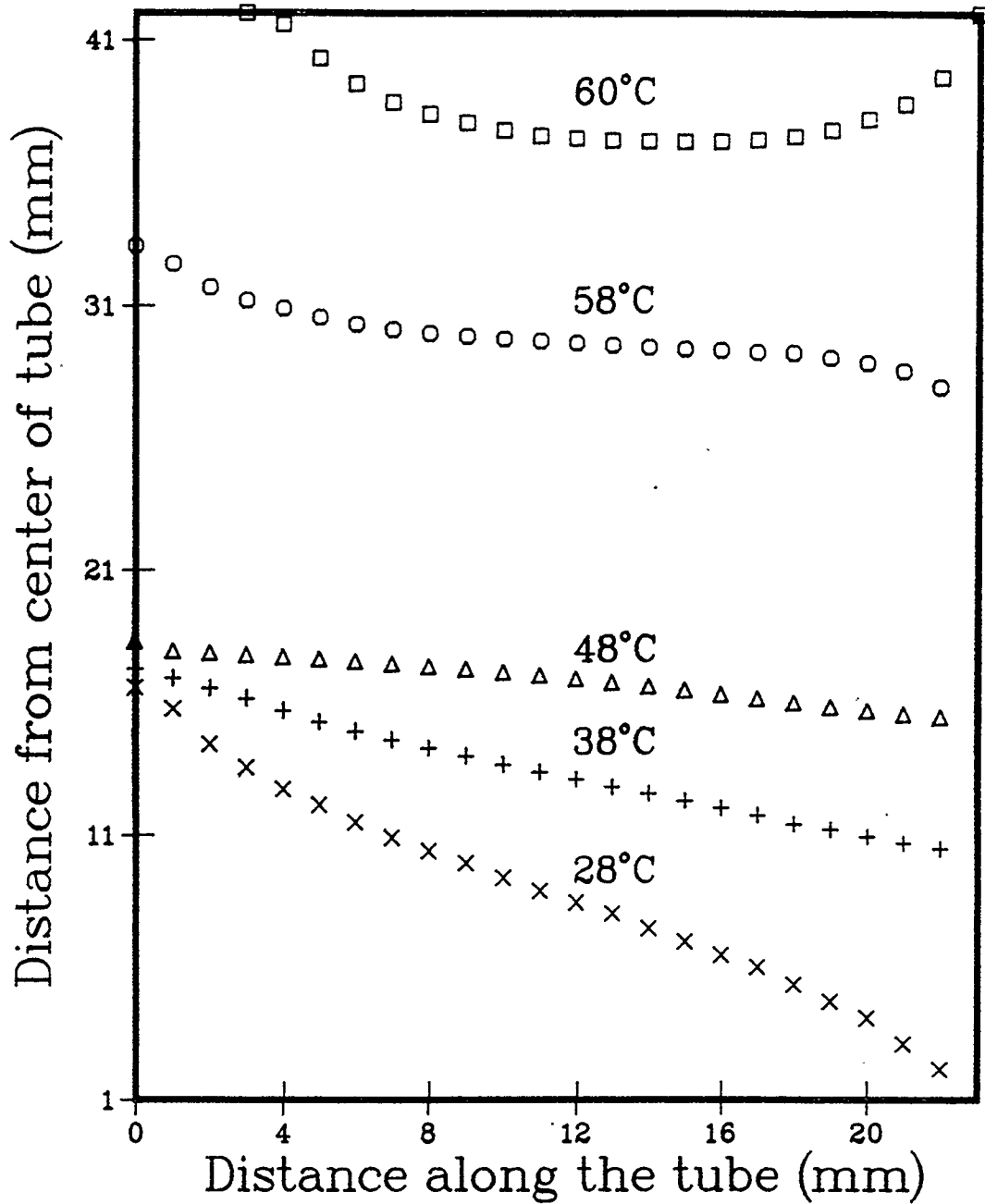


Figure 22. Plot of isothermal lines,  
 $T_c=20^\circ\text{C}$ ,  $t=16$  min.,  $p=23$  mm.,  
 $Q=7.03 \cdot 10^{-5} \text{m}^3/\text{s}$ .

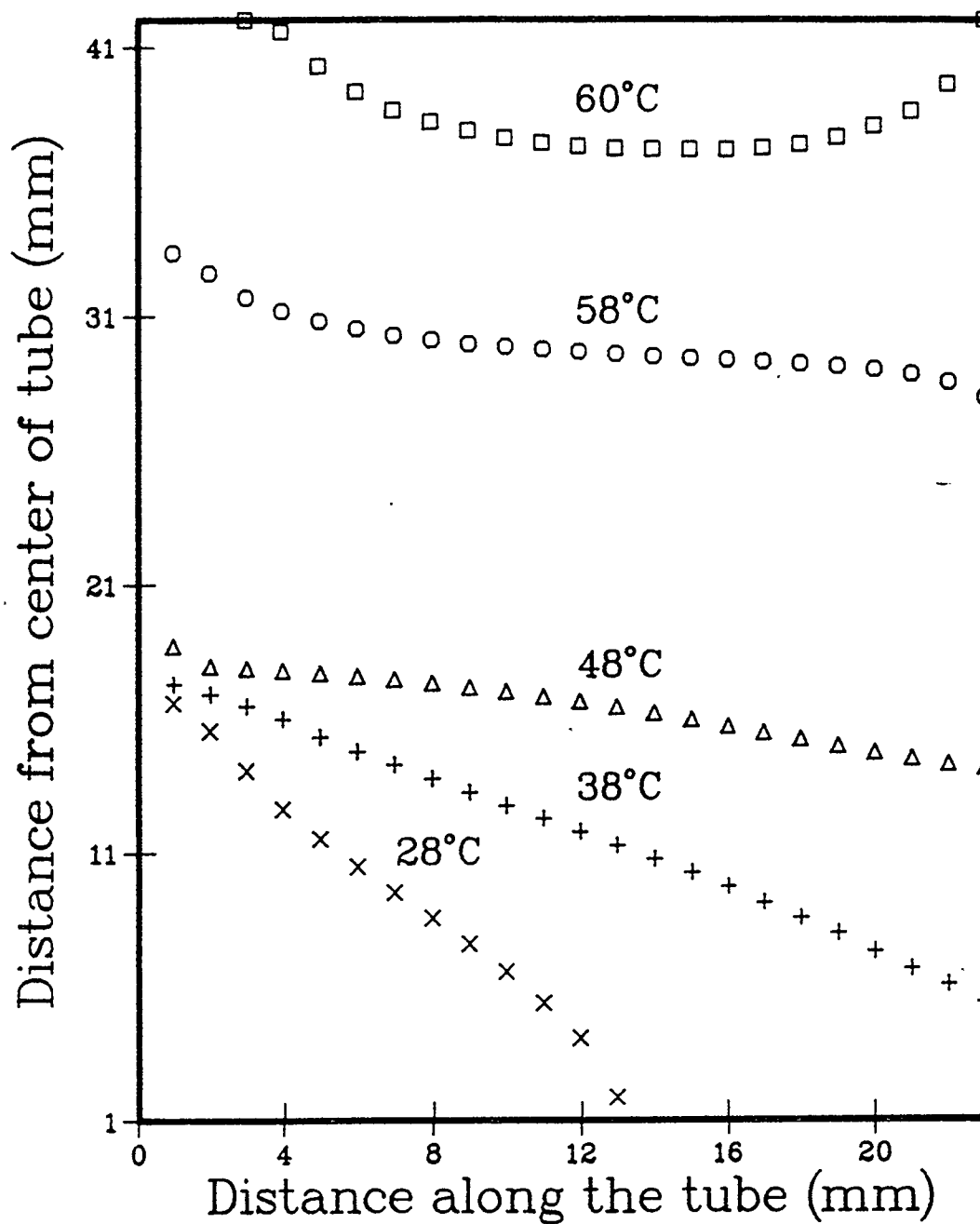


Figure 23. Plot of isothermal lines,  
 $T_c=20^\circ\text{C}$ ,  $t=16$  min.,  $p=23$  mm.,  
 $Q=3.02 \cdot 10^{-5} \text{m}^3/\text{s}$ .

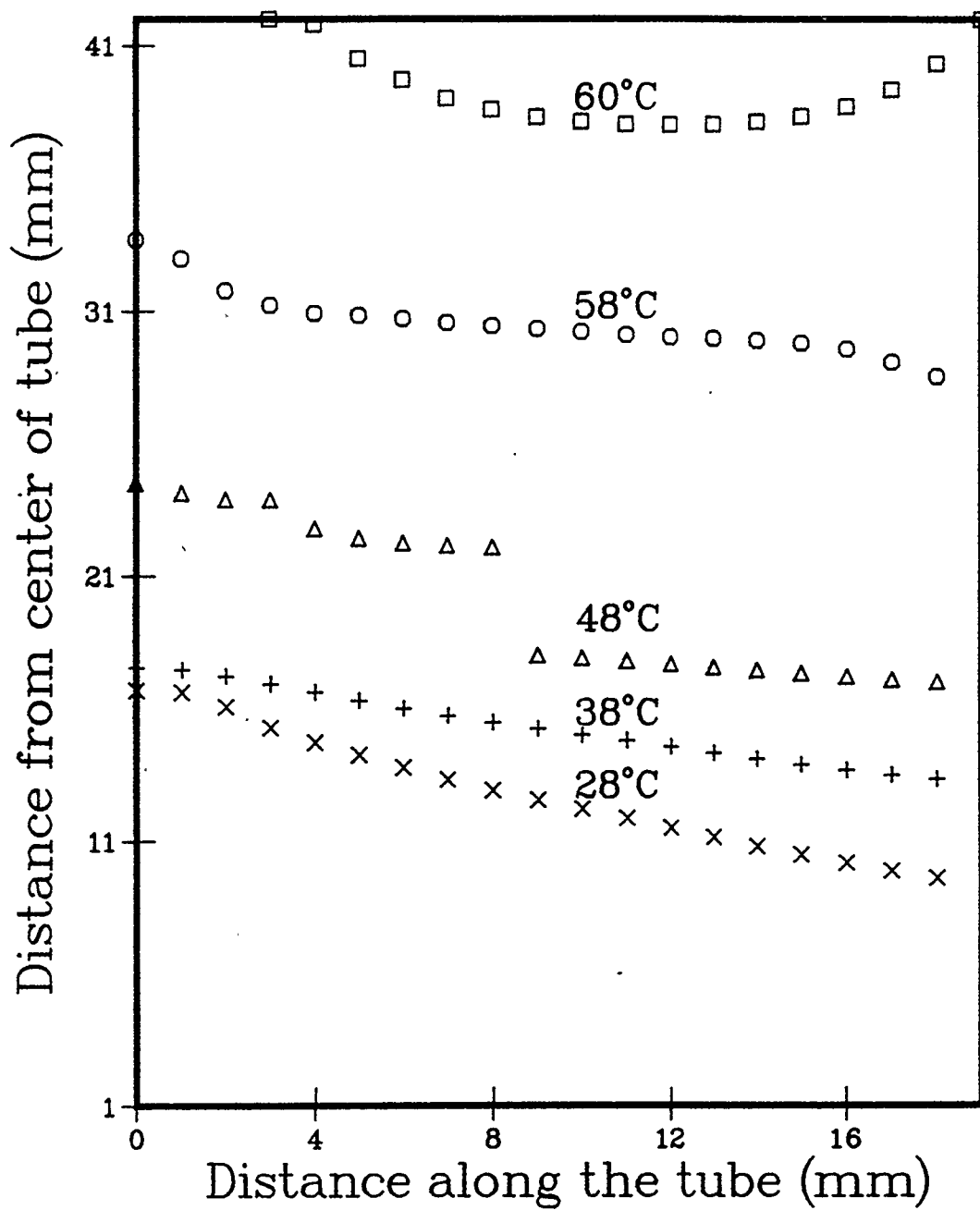


Figure 24. Plot of isothermal lines,  $T_c=10^\circ\text{C}$ ,  $t=16$  min.,  $p=19$  mm.

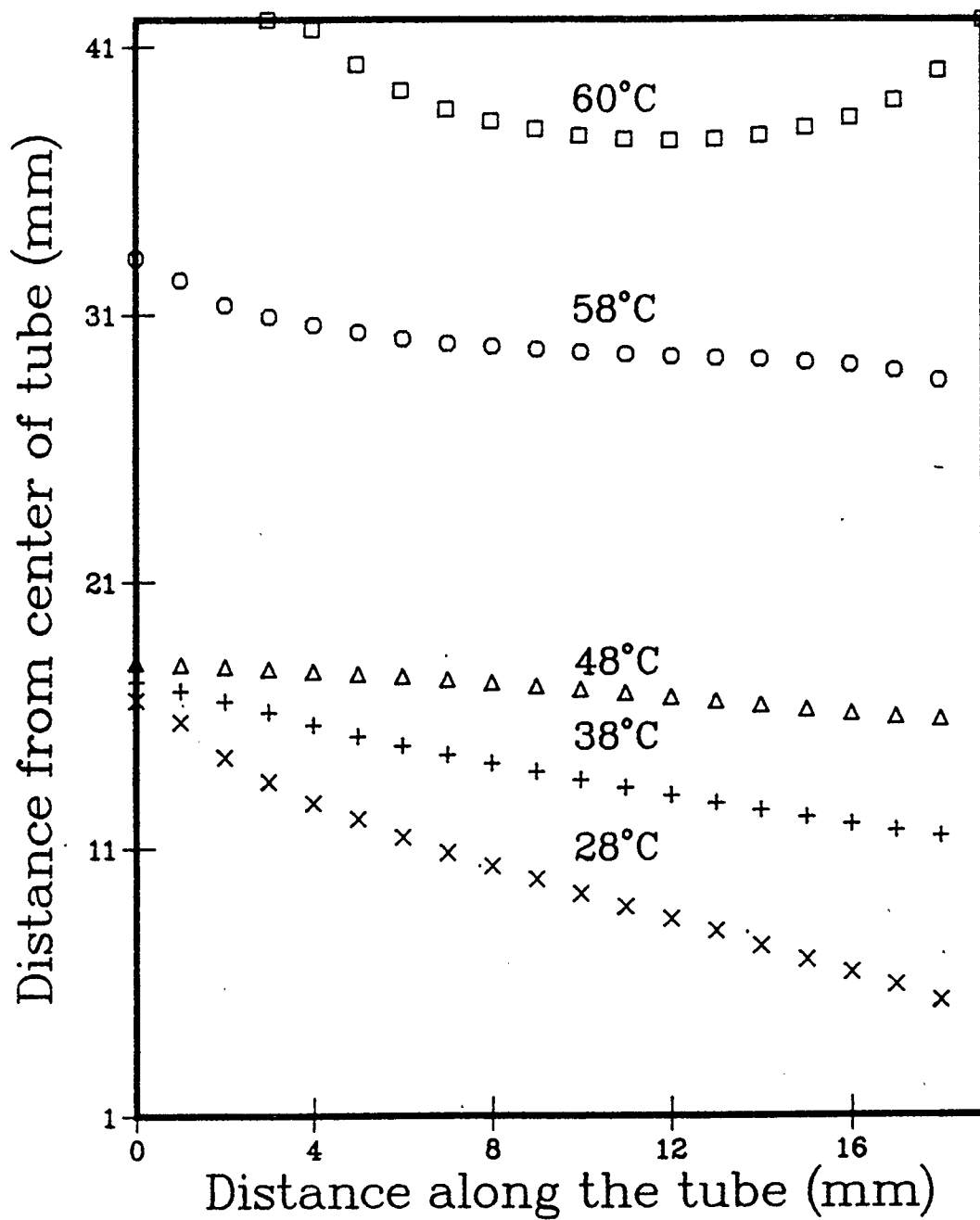


Figure 25. Plot of isothermal lines,  $T_c=20^\circ\text{C}$ ,  $t=16$  min.,  $p=19$  mm.

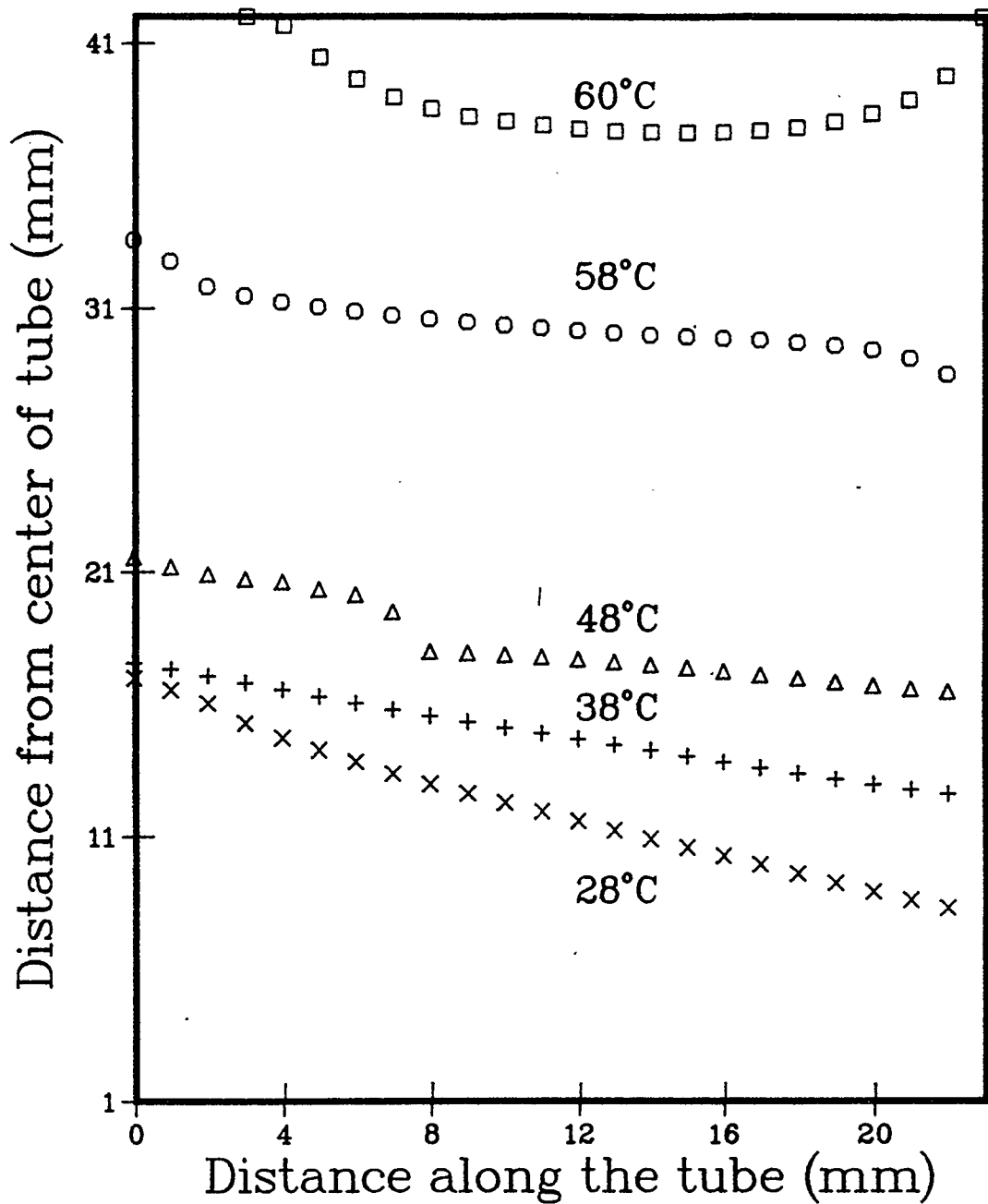


Figure 26. Plot of isothermal lines,  
 $T_c=10^\circ\text{C}$ ,  $t=16$  min.,  $p=23$  mm.,  
 $Q=7.03 \cdot 10^{-5} \text{m}^3/\text{s}$ .

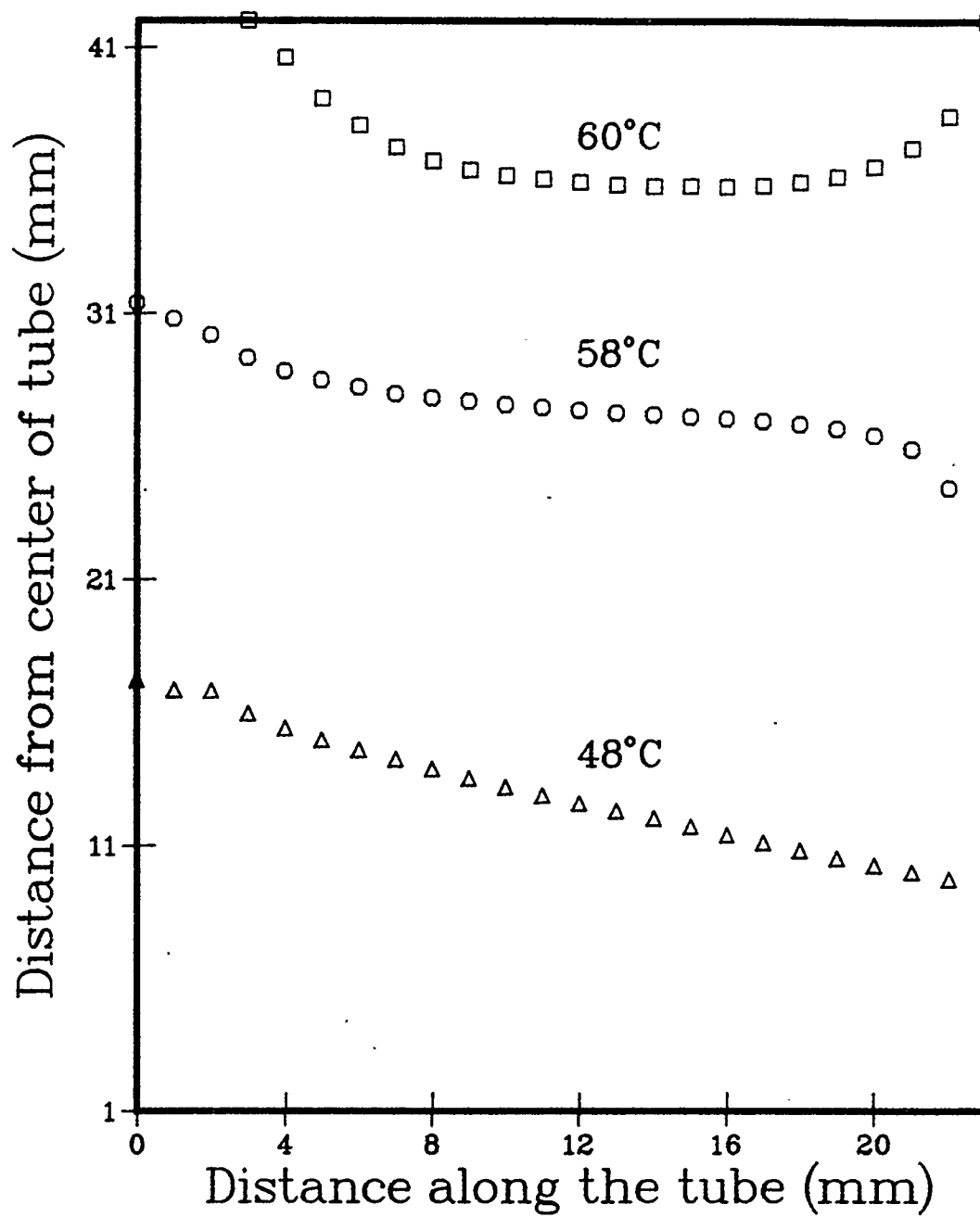


Figure 27. Plot of isothermal lines,  $T_c=40^\circ\text{C}$ ,  $t=16$  min.,  $p=23$  mm., water as a coolant.

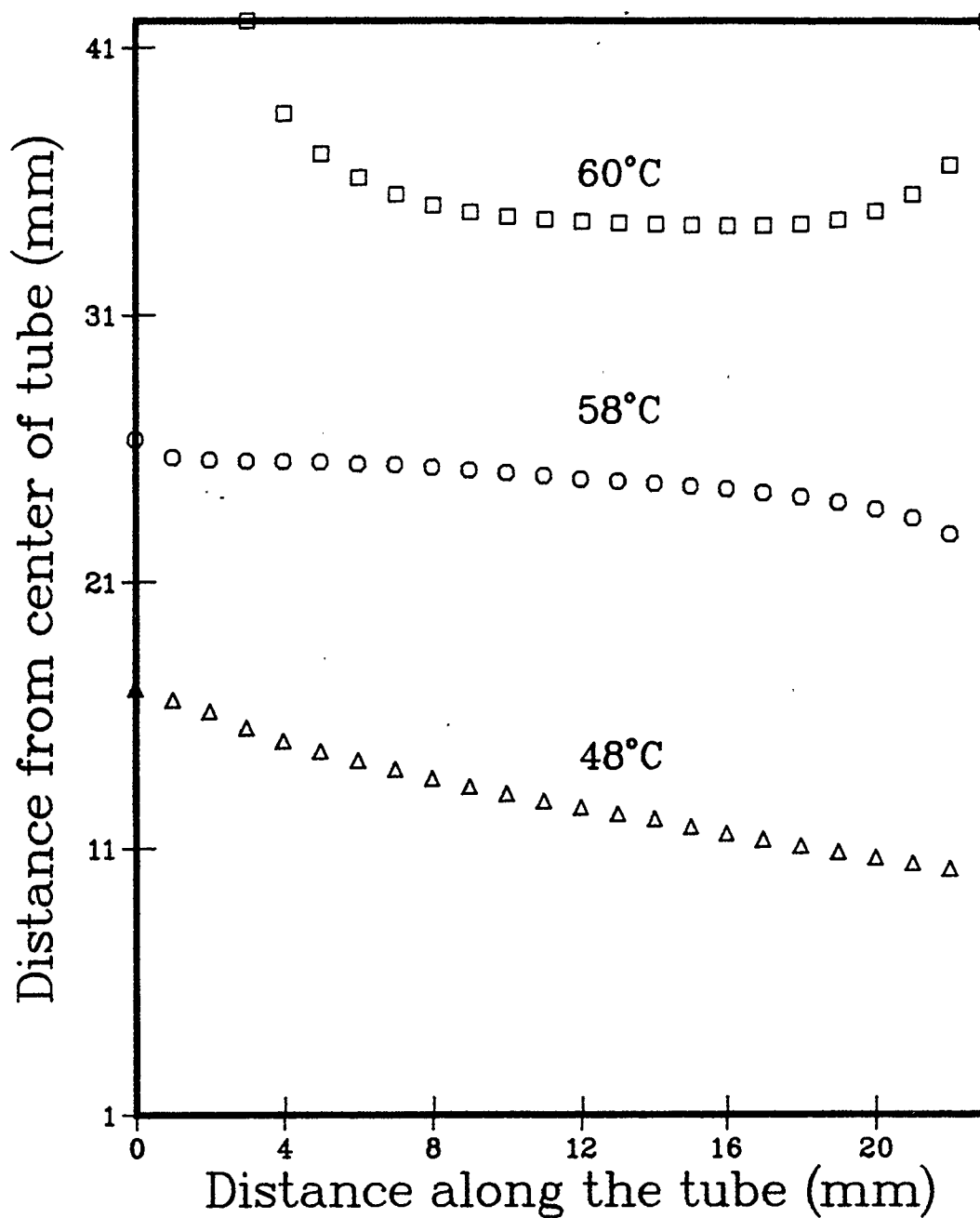


Figure 28. Plot of isothermal lines,  $T_c=40^\circ\text{C}$ ,  $t=16$  min.,  $p=23$  mm., ethylene glycol as a coolant.

the water. This sharp change in slope is explained by the temperature gradient between the metal-water interface and the water.

In order to study the effect of coolant on isothermal lines, model predictions were generated for water and ethylene glycol. The inlet temperature of each coolant was  $40^{\circ}\text{C}$ . The results for water are shown in Figure 27 and those for ethylene glycol are shown in Figure 28. The  $58^{\circ}\text{C}$  and  $60^{\circ}\text{C}$  isothermal lines of Figure 27 are located further away from the centre of the tube than those of Figure 28. The location of the  $48^{\circ}\text{C}$  isothermal line of both figures do not differ very much. The difference in the location of the isothermal lines of Figures 27 and 28 is explained by the thermophysical properties of the above mentioned coolants.

### 3.8 Estimation of the Amount of Solid Formed.

In order to study the practical importance and potential application of this model, the amount of solid formed around the tube was estimated numerically. This was necessary since the amount of solid formed is directly related to the practical importance and the potential application of this model. The predicted amount of solid formed for a given time interval is also necessary for the desublimer design.

To estimate the amount of solid formed for each case, the volume occupied by the solid layer around the tube was calculated by

differential calculus and then converted to mass. This was carried out based on the assumption that there are no void spaces between the solid layers. The entire volume of solid around the tube for each case study was divided into a fixed number of discs and the volume of each disc was calculated. The total volume was then estimated by summing up the volumes of the discs. The mass of solid formed was then estimated by the expression below.

$$\text{mass of solid formed} = \rho_s \sum_{v=1}^{20} v_v \quad (51)$$

The estimated amount of solid formed for different case studies is presented in tables 1, 2 and 3.

**Table 1. Comparison of Estimated Mass of Solid Formed for Different Tube Materials (including fins).**

Thermal Diffusivity, $\alpha_m$ ( $\text{m}^2/\text{s}$ )	$1.69 \times 10^{-5}$	$1.08 \times 10^{-5}$
Mass of solid formed (g)	42.60	39.24

**Table 2. Comparison of Estimated Mass of Solid Formed for Different Flow Rates of Water,  $T_c = 20^\circ\text{C}$ .**

Volumetric Flow Rate, Q ( $\text{m}^2/\text{s}$ )	$7.03 \times 10^{-5}$	$3.02 \times 10^{-5}$
Mass of solid formed (g)	42.60	41.08

Table 3. Comparison of Estimated Mass of Solid Formed for Different Coolants

$T_c$ ( $^{\circ}\text{C}$ )	10			20			40		
Coolant	Water	Ethylene glycol	o-xylene	Water	Ethylene glycol	o-xylene	Water	Ethylene glycol	o-xylene
Mass of solid formed (g)	43.67	38.78	35.58	42.60	37.56	33.90	37.41	33.13	28.55

CHAPTER FOUR  
CONCLUSIONS AND RECOMMENDATIONS

4.1 Conclusions

The following conclusions can be made based on the numerical modelling studies:

- (i) The numerical model developed in this thesis eliminates the inherent difficulties in formulating and applying analytical methods for desublimation problems on straight finned tubes with practically important boundary conditions.
- (ii) A numerical model for recovering sublimation products was developed which includes a new technique to make the model stable for any initial thickness of solid used to begin the computations. Model solutions were generated for different cases. In each case, the model predicted the location of the solid-gas interface, temperature distribution in the system, and mass of solid formed.
- (iii) By considering the rate of mass flux of the desubliming component at the solid-gas interface, it was possible to predict the type of desublimation applicable by evaluating the rate of desublimation.

- (iv) The type of coolant and inlet temperature of the coolant were found to be key parameters for the recovery of sublimation products.
- (v) The properties (composition and velocity) of the vapour-gas mixture and physical properties of the desubliming component were found to have a drastic effect on the rate of desublimation.
- (vi) Fin geometry and the flow rate of the coolant play important roles in recovering sublimation products.

#### 4.2 Recommendations

- (i) Model predictions are to be compared with experimental results to assess the potential application of this method.
- (ii) Investigation of the crystal structure and properties of the phthalic anhydride formed and the influence of these properties on the efficiency of recovery should be studied.
- (iii) All phenomena associated with the boundary layer were not considered in this thesis and should be analyzed further.
- (iv) The model does not account for the effect of pressure drop and arrangements of finned tubes on recovery and this should be considered.

## REFERENCES

- Amitin, A.V., Gorelik, A.G., Gevorkyan, A.A. and Ermakova, M.P.:  
"Effect of the Composition of Contact Gases on the Efficiency of  
Phthalic Anhydride Desublimation", Khim. Prom-st. 7, 428-429  
(1980).
- Atthey, D.R.: "A Finite Difference Scheme for Melting Problems", J.  
Inst. Maths. Applics. 13, 353 (1974).
- Barakat, H.Z. and Clark, J.A.: "On the Solution of the Diffusion  
Equations by Numerical Methods", J. Heat Transfer 88c, 421-427,  
(1966).
- Beech, G. and Lintonbon, R.G.: "Measurement of Sublimation Enthalpies  
by Differential Scanning Calorimetry", Thermochemica Acta 2, 86-88  
(1971).
- Bird, R.B., Stewart, W.E. and Lightfoot, E.N.: Transport Phenomena, 3rd  
Ed., McGraw-Hill, N.Y., (1960).
- Brian, P.L.T.: "A Finite Difference Method of High-Order Accuracy for  
the Solution of Three-Dimensional Transient Heat Conduction  
Problems", A.I.Ch.E.J., 7, 367-370 (1971).
- Briggs, D.E. and Young, E.H.: "Convection Heat Transfer and Pressure  
Drop of Air Across Triangular Pitch Banks of Finned Tubes", Chem.  
Engg. Prog. Symp. Ser., 59; 1 (1963).
- Bonacina, C. and Comini, G.: "On The Solution of the Nonlinear Heat  
Conduction Equations by Numerical Methods", Int. J. Heat Mass  
Transfer 16, 581-589 (1973).

- Carr, N.L., Kobayashi, R. and Burrows, D.B.: "Viscosity of Hydrocarbon Gases Under Pressure", Trans., AIME 201, 264-272 (1954).
- Carslaw, H.S. and Jaeger, J.C.: "Conduction of Heat in Solids", Oxford at the Clarendon Press, N.Y. (1957).
- Cheung, F.B. and Epstein, M.: "Solidification and Melting in Fluid Flow", Advances in Transport Processes, 3, 37-118, Wiley Eastern, N.Y. (1984).
- Crank, J. and Nicolson, P.: "A Practical Method for Evaluation of Solutions for Partial Differential Equations of the Heat Conduction Type", Proc. Camb. Phil. Soc. 43, 50-67 (1947).
- Crooks, D.A. and Feetham, F.M.: "The Vapour Pressure of Phthalic Anhydride", J. Chem. Soc., 899, (1946).
- Crowley, A.B.: "Numerical Solution of Stefan Problems", Int. J. Heat Mass Transfer 21, 215, (1978).
- Dankwertz, P.V.: "Unsteady State Diffusion or Heat Conduction With Moving Boundaries", Trans. Faraday Society, 46, 701, (1950).
- Douglas, J. and Rachford, H.H.: "On the Numerical Solution of Heat Conduction Problems in Two and Three Space Variables", Trans. Am. Math. Soc. 82, 421-439, (1956).
- Forster, C.A.: "Finite Difference Approach to Some Heat Conduction Problems Involving Change of State", Report to the English Electric Company, Luton, England (1954).
- Goodman, T.R.: "The Heat Balance Integral and Its Application to Problems Involving a Change of Phase", Trans. ASME, 80, 335, (1958).

- Goodrich, L.E.: "Efficient Numerical Technique For One-Dimensional Thermal Problems with Phase Change", Int. J. Heat Mass Transfer 21, 615-621, (1978).
- Gorelik, A.G., Amitin, A.V. and Ermakov, M.P.: "Mathematical Modeling of Desublimation in Tubular Apparatus", Teor. Osn. Khim., Tekhnol. 14, 825-836 (1980).
- Grebenyuk, A.F., Korobchanskii, V.I. and Korobchanskii, Yu. V.: "Continuously Operating Condenser for the Freezing of Phthalic Anhydride", Koks i Khim., 7, 59-61 (1981).
- Gutowski, R.: "The Problem of Motion of the Freezing Front in Liquids", Archiwum Mechaniki Stosowanej, 15, 167 (1963).
- Gutowski, R.: "The Motion of the Freezing Front in a Liquid Taking into Account The Dependency of Thermal Parameters on the Temperature", Archiwum Mechaniki Stosowanej, 16, 49 (1964).
- Hastaoglu, M.A.: "A Numerical Solution to Moving Boundary Problems - Application to Melting and Solidification", Int. J. Heat Mass Transfer 29, 495-499 (1986).
- Hastaoglu, M.A.: "Numerical Solution of a Three-Dimensional Moving Boundary Problem: Melting and Solidification with Blanketing of a Third Layer", Chem. Eng. Sc. 42, 2417-2423 (1987).
- Janz, G.J.: Thermodynamic Properties of Organic Compounds. Estimation Methods, Principles and Practice, Academic Press, N.Y. 113 (1967).
- Jakob, M.: Heat Transfer, Vol. 1, John Wiley & Sons, Inc., N.Y. (1949).
- Kays, W.M.: "Numerical Solutions for Laminar-Flow Heat Transfer in Circular Tubes", Trans. ASME 77, 1265-1274 (1955).

- Krupiczka, R. and Bilik, J.: "Heat Transfer in the Process of Sublimational Condensation (Desublimation) of Phthalic Anhydride. I. Experiments and Model of the Process", *Inz. Chem.* 10, 93-106 (1980).
- Krupiczka, R. and Bilik, J.: "Heat Transfer in the Process of Sublimational Condensation (Desublimation) of Phthalic Anhydride. II. Experimental Results Elaborations", *Inz. Chem. Procesowa*, 10, 507-522 (1980).
- Kreith, F. and Romie, F.E.: "A Study of the Thermal Diffusion Equation With Boundary Conditions Corresponding to Solidification or Melting of Materials Initially at the Fusion Temperature", *Proceedings of the Physics Society* 68, 277, (1955).
- Landau, H.G.: "Heat Conduction in a Melting Solid", *Quart. Appl. Math.* 8, 81-94, (1950).
- Lewis, R.W. and Morgan K.: *Numerical Methods in Thermal Problems*, Pineridge Press, Swansea (1979).
- Lindsay, A.L. and Bromley, L.A.: *Ind. Eng. Chem.* 42, 1508 (1950).
- Longworth, D.: *A Numerical Method to Determine the Temperature Distribution Around a Moving Weld Pool in Moving Boundary Problems In Heat Flow and Diffusion*. Oxford University Press, Oxford, 54, (1975).
- McAdams, W.H.: *Heat Transmission*, Third Ed., McGraw-Hill, N.Y., (1954)
- Masliyah, J.H. and Nandakumar, K.: "Heat Transfer in Internally Finned Tubes", *J. Heat Transfer* 98, 257-261, (1976).

- Meyer, G.H.: "Multidimensional Stefan Problems", J. Num. Anal. 10, 522 (1973).
- Murray, R.W. and Landis, F.: "Numerical and Machine Solutions of Transient Heat Conduction Problems. I. Methods of Analysis and Sample Solutions", J. Heat Transfer, 81, 106-112 (1958).
- Mori, S., Sakakibara, M. and Tanimoto, A.: "Steady Heat Transfer to Laminar Flow in a Circular Tube with Conduction in the Tube Wall", Heat Transfer - Jpn. Res. 3, 37-46, (1974).
- Neel, C.B. Jr.: "An Investigation Utilizing an Electric Analogue of Cyclic De-Icing of a Hollow Steel Propeller with an External Blade Shoe", NACA, TN 2852, (1952).
- Nord, M.: "Sublimation", Chem. Eng., 58, 157 (1951).
- O'Brien, G.C., Hyman, M.A. and Kaplan, S.: "A Study of the Numerical Solution of Partial Differential Equations", Journal of Mathematics and Physics, 29, 223 (1951).
- Ockendon, J.R. and Hodkins, W.R.: Moving Boundary Problems in Heat Flow and Diffusion. Oxford University Press, Oxford (1975).
- Otis, D.R.: "Solving the Melting Problem Using the Electric Analogy of Heat Conduction", Heat Transfer and Fluids Mechanics Institute, Stanford University, 29 (1956).
- Ozisik, M.N.: "A Note on the General Formulation of Phase Change Problem as Heat Conduction Problem with a Moving Heat Source", J. Heat Transfer, 100c, 370-371 (1978).
- Ozisik, M.N.: Heat Conduction, Wiley Interscience, Toronto (1980).

- Pham, T.K.: "A Fast Unconditionally Stable Finite-Difference Scheme for Heat Conduction with Phase Change", *Int. J. Heat Mass Transfer* 28, 2079-2084 (1985).
- Price, P.H. and Slack, M.R.: "The Effect of Latent Heat in Numerical Solutions of the Heat Flow Equations", *British Journal of Applied Physics*, 5, 285, (1954).
- Redozubov, D.B.: "The Solution of Linear Thermal Problems with a Uniformly Moving Boundary in a Semiinfinite Region", *Soviet Physics - Technical Physics*, 5, 570 (1960).
- Reid, R.C. and Sherwood, T.K.: *The Properties of Gases and Liquids*, McGraw-Hill, N.Y., (1977).
- Saitoh, T.: "Numerical Method for Multidimensional Freezing Problems in Arbitrary Domains", *Trans. ASME*, 100, 294-299, (1978).
- Sanders, R.W.: "Transient Heat Conduction in a Melting Finite Slab", *ARS J.*, 30, 1030 (1960).
- Sapozhnikov, V.V.: "Use of a Gas-Dust Heat Transfer Agent in the Manufacture of Phthalic Anhydride", *Zh. Khim* 21, 242, (1974).
- Shamsundar, N. and Sparrow, E.M.: "Analysis of Multidimensional Conduction Phase-Change Via the Enthalpy Model", *J. Heat Transfer* 97, 333-340 (1975).
- Smittle, D.: "Maximize Heat Recovery from Hot Flue Gas with Finned Tubing", *Power*, 76, (Aug. 1980).
- Springer G.S. and Olson, D.R.: "Method of Solution of Axisymmetric Solidification and Melting Problems", *ASME* 62, 246, (1962).

- Stynes, S.K. and Myers, J.E.: "Transport from Extended Surfaces",  
A.I.Ch.E.J., 10, 437 (1964).
- Sunderland, J.E. and Grosh, R.J.: "Transient Temperature in a Melting  
Solid", ASME, J. of Heat Transfer, 83, 409, (1961).
- Surovtsev, V.V. and Trubkin, V.E.: "Enthalpy - Concentration Diagram  
for the Air-Phthalic Anhydride System", Zh. Khim. 13, 825 (1975).
- Treybal, R.E.: Mass Transfer Operations, 3rd Ed., McGraw-Hill, N.Y.  
(1980).
- Trezek, G.J. and Witmer, J.G.: "Finite-Difference Methods for  
Inhomogeneous Regions", J. Heat Transfer 94c, 321-323 (1972).
- Voller, V. and Cross, M.: "An Explicit Numerical Method to Track a  
Moving Phase Change Front", Int. J. Heat Mass Transfer 26, 147-150  
(1983).
- Vogel, H.: Ann. Physik, 43, 1235 (1914).
- Von Glahn, V.H.: The Icing Problem - Current Status of NACA Techniques  
and Research, AGARD, Papers presented at the Seventh Meeting of  
The Wind Tunnel and Model Testing Panel, 293 (1955).
- Von Rosenberg, D.U.: Methods for the Numerical Solution of Partial  
Differential Equations. Elsevier, N.Y. (1969).
- Weierman, C.: "Guidelines for Selecting Finned Tubes", Oil Gas J., 64,  
(Nov. 1975).
- Young, D.M.: "Iterative Methods For Solving Partial Differential  
Equations", Trans. Am. Math. Soc., 92-111, (1954).